NASA Technical Memorandum 101406

Structural Dynamics Branch Research and Accomplishments for FY 1988

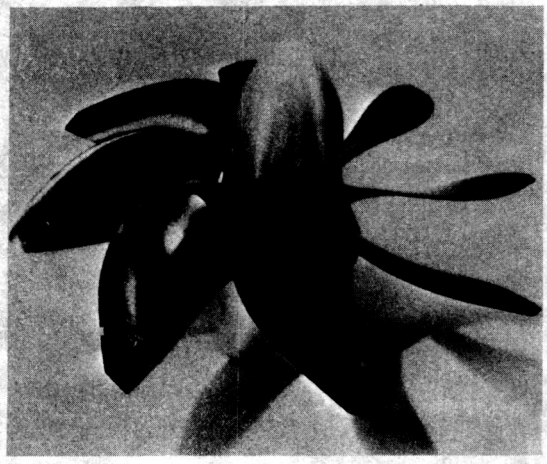

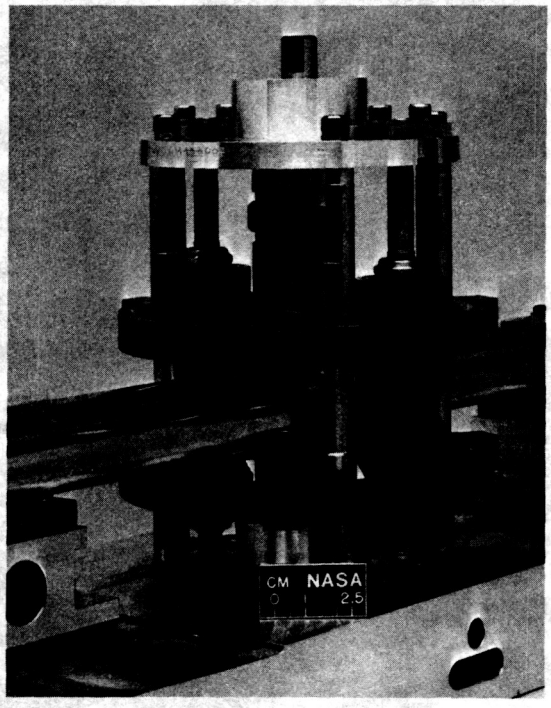

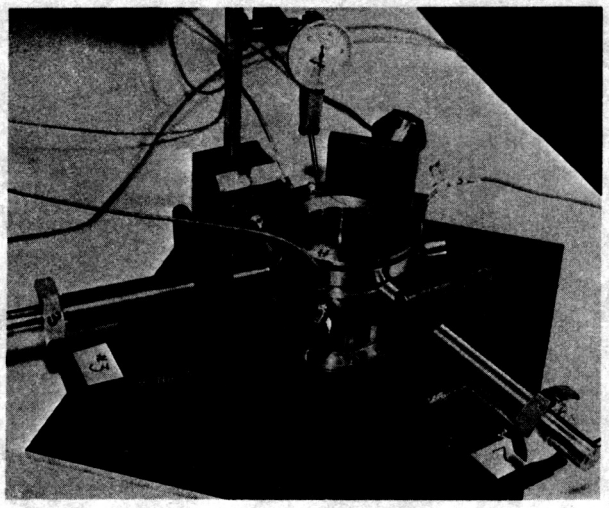

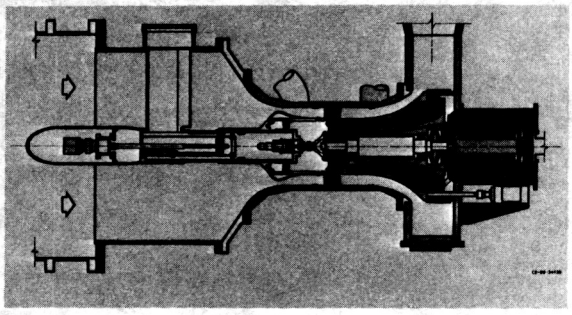

NASA

April 1989
Lewis Research Center

NASA Technical Memorandum 101406

Structural Dynamics Branch Research and Accomplishments for FY 1988

Lewis Research Center
Cleveland, Ohio

April 1989

National Aeronautics and
Space Administration

**Scientific and Technical
Information Branch**

Preface

This document summarizes some of the technical accomplishments of the Structural Dynamics Branch of NASA Lewis Research Center for fiscal year 1988. Included is the work of our in-house researchers, contractors, and grantees since they have achieved significant results throughout the year.

The Structural Dynamics Branch conducts research dealing with advanced propulsion and power systems as well as precision mechanical systems. Our work directly supports NASA's turboprop, space experiments, space shuttle main engine (SSME), National Aerospace Plane (NASP), supersonic fan, space station, and space power programs. This work can be broadly classified into four major activities: turbomachinery aeroelasticity, turbomachinery vibration control, dynamic systems response and analysis, and computational structural methods.

In aeroelasticity, we are developing improved analytical and experimental methods for avoiding flutter and minimizing forced vibration response of aerospace propulsion systems. Work elements include classical (frequency domain) methods, time-domain methods, computational methods for fluid-coupled structural response, experimental methods, and application studies (turboprop, turbofan, turbopump, and advanced core technology). The new year brings an increased emphasis on the problems associated with supersonic throughflow-fan aeroelasticity, the forced vibration response of SSME class turbomachinery blading, and counter-rotating propfan systems.

In vibration control, we are conceiving, analyzing, developing, and demonstrating new methods to control vibrations in aerospace systems to increase life and performance. Work elements include actively controlled structures, passive vibration control methods, computational methods for active vibration control, and application studies (vibration isolation, magnetic and piezoactively controlled bearings, and cryoturbomachinery). This area continues to be a major focus for us. Methods for unbalance control, critical speed control, and direct control of transient instabilities in rotating equipment are being developed. New approaches for magnetic and piezoelectric actuators are being developed along with a variety of adaptive real-time digital, analog, and hybrid control strategies.

In dynamic systems, we are analyzing and verifying the dynamics of interacting systems as well as developing concepts and methods for motion control in microgravity environments. Work elements include microgravity robotic systems, parameter identification methods, computational methods for dynamics analysis, and application studies (space lab mechanisms and robotics, NASP engine sealing concepts, and parallel computing for dynamics analysis). Growing from this program is an increased emphasis on the basic technology needs for space-based mechanisms. Requirements for precise, reliable long-life space-based mechanisms are increasingly important. We are developing technology for reactionless mechanical actuators, precision roller-driven joints for robot arms and other space-based rotary joints, high-speed actively controlled bearings for space-based propulsion and pumping systems, and methods to evaluate these new technologies.

Our work in computational methods is no longer considered a separate activity. Rather, computational methods development has been folded in with the objectives of the three other major focus areas within the branch. The goal of this work is to fundamentally improve the use of modern computers for the solution of realistic structural dynamics problems, with a particular emphasis on parallel processing. In aeroelasticity, computational methods work is focused on time-domain solutions and coupled fluid structure interaction. In vibration control, the computational methods are focused on individual bearing control, hierarchical schemes for controlling the response of distributed elastic shaft systems, and magnetic vibration isolation of space experiment platforms. In dynamic systems, the focus is on new algorithms for structural dynamics analysis.

I am personally excited by the progress we have made and the new directions we are heading. I am looking forward to next year's accomplishments and to introducing next year's report.

L.J. Kiraly
Branch Manager

Contents

Turbine Engine Transient and Steady-State Analysis

In the NASA Lewis Research Center sponsored Turbine Engine Transient Analysis (TETRA) program, a computational tool was developed to predict the transient dynamic response of engineering structures to suddenly applied loads, such as from the loss of a blade. This tool was improved by adding two modules: (1) the flexible bladed disk and (2) the squeeze film bearing. The latter was added by Case Western Reserve University under NASA Lewis sponsorship.

To synthesize the model, we constructed the dynamic response of a complex structure in terms of the natural modes of its principal structural components. The equations of motion in the modal generalized coordinates were solved numerically by central difference integration in the time domain. This solution has the flexibility to accommodate nonlinearities, such as tip rubs, squeeze films or other nonlinear bearings or connecting elements. In addition, the gyroscopic coupling between motions in the vertical and horizontal planes of rotating structures is considered for rigid as well as flexible bladed disks.

The transient response of a structure is a history of the motion and loads which initially vary nonuniformly in time until a steady-state condition is reached. Where damping is low and modal frequencies are high, the time steps required to reach steady state can be numerous. For this reason, a more direct method to calculate steady-state response was undertaken.

Steady-state capability allows the forced response amplitudes to be calculated as a function of excitation frequency so that engine response from a sinusoidal input, such as unbalance, can be obtained over the engine operating speed range. For purely linear systems, the methodology is well established. However, in the presence of nonlinearities, obtaining a steady-state solution is neither simple nor straightforward. This is especially true with large systems of equations with strong nonlinearities.

To produce a more pragmatic solution to this complex and important problem, the calculation is limited to the first harmonic of the forcing frequency. Solution by iteration of the compatibility conditions, at only the nonlinear connecting elements, dramatically reduces the number of equations to be solved. The method of harmonic balance originated by Kryloff and Bogoliuboff was used to transform the nonlinear differential equations to a system of nonlinear connections.

This methodology was implemented in a computer code built on the original TETRA program (figs. 1, 2,

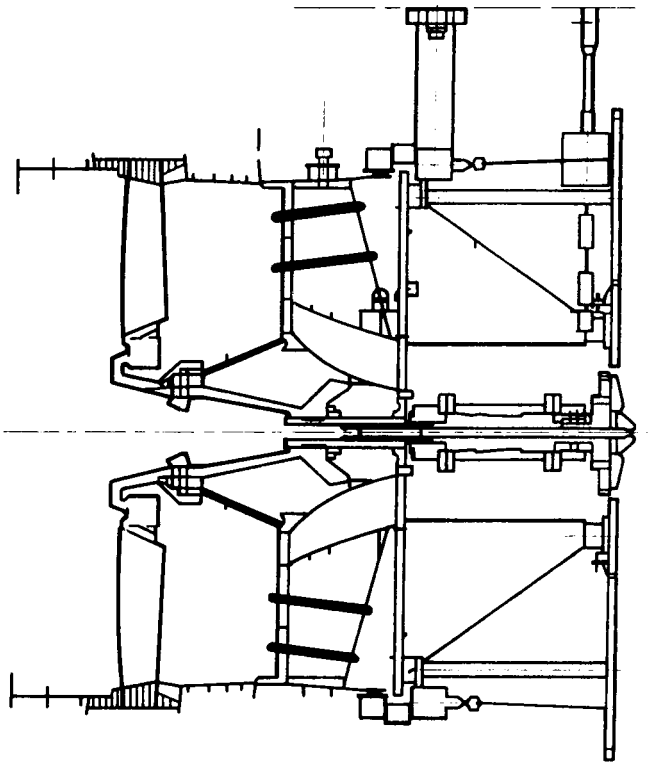

Figure 1.—Blade-out test vehicle cross section.

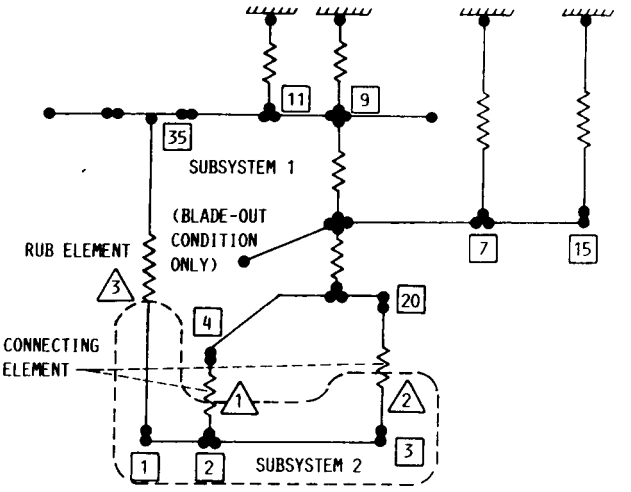

SUBSYSTEM	NUMBER OF MODES USED	SPEED, RPM
1	13	424 TO 75 86/
2	4	46 TO 78 001

Figure 2.—Blade-out test vehicle TETRA schematic.

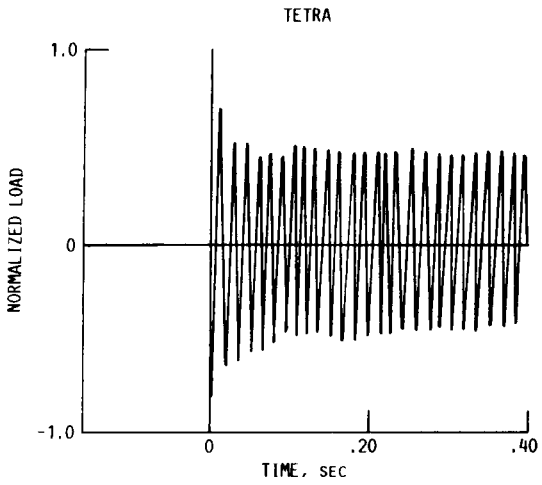

Figure 3.—Blade-out response data.

and 3). The new program, TETRA 2, has the capability of the original transient analysis as well as the steady-state solution. To make TETRA 2 user friendly, the inputs of the original TETRA program have been changed as little as possible.

The NASA-sponsored TETRA 2 computer code provides industry with a comprehensive turbine engine rotordynamics computer code that can be used to calculate both transient and steady-state responses. The nonlinear capability of the program greatly enhances and broadens its application to a more realistic analysis of real engines.

Researchers: V. Gallardo and G. Black (General Electric).
Technical monitor: C. Lawrence (NASA Lewis).

Transient Finite Element Analysis on the Transputer System

Many large-scale computer simulations involve such an enormous number of computations that they are too time consuming for even today's supercomputers. To achieve large increases in computational speed, researchers have focused on parallel-processing computers. Parallel-processing computers are composed of two or more interconnected processors. For parallel computations, a task is divided into subtasks that are performed independently on separate processors.

This study used a parallel-processing computer for the analysis of dynamic finite element problems. Direct-time integration methods are the methods most useful for the analysis of dynamic problems because they are applicable to nonlinear structural problems. Some examples of nonlinear problems are structures with large displacements and structures composed of a nonlinear material. With direct methods, the time period of interest is split into small steps and the solution is computed at each time step. In some nonlinear problems, a new system of equations must be solved at every step. The solution of such problems can be too time consuming if many time steps are needed or if a large system of equations must be solved. For example, three-dimensional finite element problems can have several hundred thousand equations. For this reason, parallel processing is being investigated as a means of speeding-up this type of analysis.

In this study, the central difference method was chosen for the time integration rule. Since this is an explicit method, the displacement at different nodes of the finite element mesh can be computed independently of each other over a time step. This allows the finite element problem to be partitioned into subproblems that are solved on different processors. A system of transputer microprocessors was used for the computations.

A one-dimensional bar problem, shown in figure 4, was analyzed using a parallel algorithm. The bar was divided into subproblems, which were assigned to different processors. Information was exchanged between the processors after every time step. Table I gives the solution times for two problems of different sizes. As can be seen from this data, doubling the number of processors decreases the computational time by nearly half.

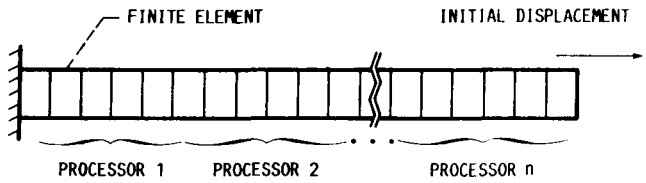

Figure 4.—Finite element model of one-dimensional bar problem. Displacement of nodal groups calculated on separate processors.

TABLE I.—SOLUTION TIMES FOR ONE-DIMENSIONAL FINITE ELEMENT PROBLEMS USING VARIOUS NUMBERS OF PROCESSORS

(a) Solution times for the 100-element problem

Number of time steps	Number of processors		
	1	2	4
	Time, sec		
1	0.13	0.07	0.40
100	1.94	1.09	.64
1000	21.66	11.75	6.55
5000	111.91	59.64	32.82

(b) Solution times for the 1000-element problem

Number of time steps	Number of processors		
	1	2	4
	Time, sec		
1	9.55	3.50	1.71
100	26.26	12.13	6.16
1000	182.45	93.02	49.99
5000	946.12	518.02	281.19

Researchers: P. Smolinski (University of Pittsburgh) and L.J. Kiraly and D.C. Janetzke (NASA Lewis).

Multifrontal Parallel Solution Method in Vibration Analysis of Finite Element Models

The multifrontal solution method offers a new parallel algorithm to solve the generalized eigenproblem, $K\Phi = M\Phi\Lambda$, typically encountered in finite element modeling of linear systems. It is based on the classical frontal solution method for simultaneous linear equations and the modified subspace method for the eigenproblem. Problems are analyzed concurrently by using each processor to create the stiffness and mass matrices of the elements located within its assigned domain and by performing simultaneous assembly/forward elimination and back substitution for each domain. The modified subspace eigenanalysis method also exploits parallelism by projecting the stiffness and mass matrices onto the required subspace in each iteration within each domain.

The multifront can be visualized as sweeping all domains concurrently in forward and then backward directions. This process can be repeated until the set of the least dominant eigenpairs of the required subspace is calculated to a specified degree of accuracy.

The parallel architecture achieves load balancing by assigning each task an equal number of elements and by numbering the elements such that the maximum width of the front is the same in all domains. The completely connected architecture allows each processor to communicate its interface matrices to all other processes.

Figure 5 shows the algorithm used to implement the parallel solution on the Cray-XMP computer at NASA Lewis. To measure the performance of the new method, we calculated computational speedup and efficiency for a number of typical problems using the two processors of the Cray-XMP computer. Speedup is defined as the ratio of the clock time used for sequential solution to the clock-time used in parallel solution. The sequential solution used for comparison is also based on the frontal and the subspace methods. Computational efficiency is determined by dividing the speedup by the number of processors.

Table II shows a summary of the results obtained to date in a dedicated processing environment on the Cray-XMP computer running under the COS operating system. Efficiency and speedup of up to 92 percent and 1.85, respectively, have been realized. Overhead due to communication links between the two processors (tasks) is relatively very small for the numerical experiments examined to date in this study.

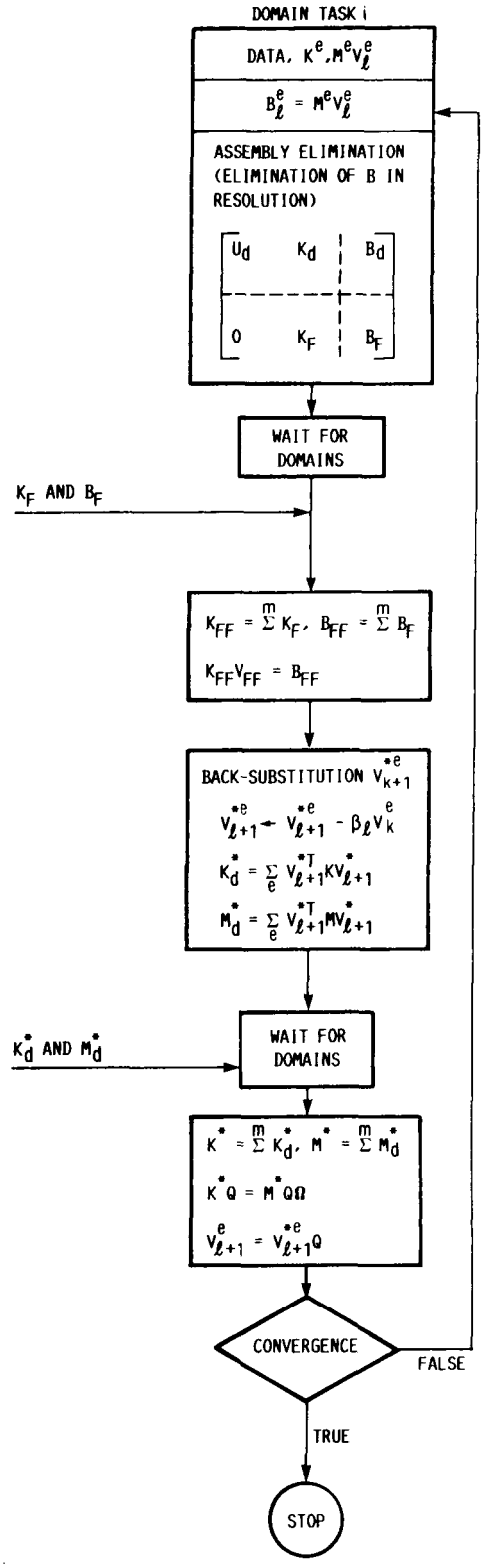

Figure 5.—Parallel algorithm for ith domain.

TABLE II.—COMPUTATIONAL SPEEDUP AND EFFICIENCY USING TWO PROCESSORS

Type	Number of elements	Number of DOF's[a]	Number of eigenpairs	Speedup	Efficiency, percent
Beam (clamped at both ends)	500	1503	4	1.85	92
	20	63	4	1.49	75
Plate (clamped on all sides)	16	115	2	1.65	82
			4	1.80	90
	40	259	2	1.81	90
			4	1.66	83

[a]Degrees of freedom.

Researchers: F.A. Akl and M. Morel (Ohio University) and L.J. Kiraly (NASA Lewis).

Multi-Time-Step Transient Finite Element Analysis

Direct-time integration methods are useful for the analysis of dynamic problems because they can be applied to nonlinear problems. Direct-time integration involves splitting the time interval into small steps and computing the solution at each of these steps.

One type of direct integration method is the central difference rule, which is advantageous because it does not involve the solution of a system of equations. However, it is only conditionally stable, and the time step must be less than a critical value for meaningful results. The maximum time step is inversely proportional to the highest frequency of the system so that small elements, or elements of stiff material, reduce the maximum time step. In finite element problems, where there is a large difference in element sizes or problems composed of different materials, this method may not be feasible because the small or stiff elements require that the entire problem be integrated with a small time step.

To overcome this difficulty multi-time-step integration has been proposed. With multi-time-step integration different subdomains of the finite element mesh are integrated with different time steps. In this way, the small, or stiff elements, can be integrated with a small time step while the remainder of the elements are integrated with a larger time step, which reduces the overall computational time.

Since the multi-time-step central difference method maintains the same structure as the central difference method, no equation solving is necessary. This allows the algorithm to be easily parallelized by dividing the nodes of the finite element mesh into groups which can be solved on different processors. In this study, a system of transputer microprocessors was used for the parallel processing.

A one-dimensional bar problem composed of different size elements, shown in figure 6, was analyzed. The nodes in the bar are divided into different groups which are computed on different processors. In this problem, the nodes between the large elements use a time step 10 times larger than the other nodes. The solution time for multi-time-step and single time-step integration using different numbers of processors are given in table III. As the data indicate, multi-time-step integration can give up to a 75-percent reduction in computer time as compared to single time-step integration for the solution of the model problem.

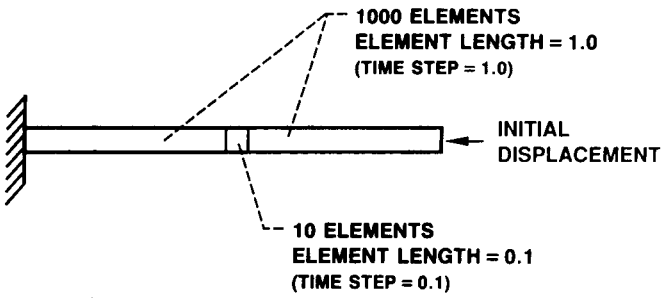

Figure 6.—One-dimensional bar finite element test problem for comparison of standard and multi-time-step integration.

TABLE III.—COMPARISON OF TEST PROBLEM SOLUTION TIMES USING SINGLE- AND MULTI-TIME-STEP INTEGRATION FOR DIFFERENT NUMBERS OF PROCESSORS

Number of processors	Time, sec		Speedup for multi-time-step method
	Single time-step integration	Multi-time-step integration	
3	227.01	77.83	2.9
5	139.64	38.53	3.6
7	97.93	25.82	3.8
9	76.40	19.53	3.9
13	51.24	12.83	4.0
17	39.59	9.91	4.0
25	27.42	7.93	3.5
33	21.49	7.41	2.9

Researchers: P. Smolinski (University of Pittsburgh) and D.C. Janetzke (NASA Lewis).

Shape Optimal Design of Elastic Bodies by Using a Mixed Variational Formulation

Shape optimal design is a problem that has interested many researchers in the last 15 years. Zienkiewicz and Campbell were among the first to approach this problem by using a virtual displacement-based finite element method. Subsequently, this method has been applied widely to problems in shape optimal design, but only with mixed success.

This study develops a variational formulation and procedure to compute an optimal design shape for two-dimensional linear elastic bodies by using a mixed finite element formulation. In some situations, mixed finite element methods provide a more accurate computation of stresses and strains at the element nodes than the virtual displacement technique. Hence, the structure at each optimization iteration is modeled more accurately and an improved structural shape results.

The optimality criterion used herein was to minimize the maximum value of the Von Mises equivalent stress (or other suitable stress measure) in the body subject to an isoperimetric constraint on the area.

In the finite element implementation of this technique, an elliptical automatic mesh generator that assured an orthogonal finite element mesh at the domain boundary was used at each shape redesign. Use of this mesh generator avoided the increase in finite element error caused by mesh distortion during shape redesign and therefore prevented the convergence instabilities experienced in previous optimization studies.

The analysis technique has been tested with several classical shape optimization problems including optimization of a hole in a square sheet. As shown in figure 7, a sheet with an initial square hole was loaded along its vertical and horizontal faces with equally distributed forces. The required hole area was specified by the user.

The optimization executes automatically, alternating between evaluating element stress-strain levels and reshaping the hole subject to the optimality criterion, until the hole's area matches the specified area within some tolerance band.

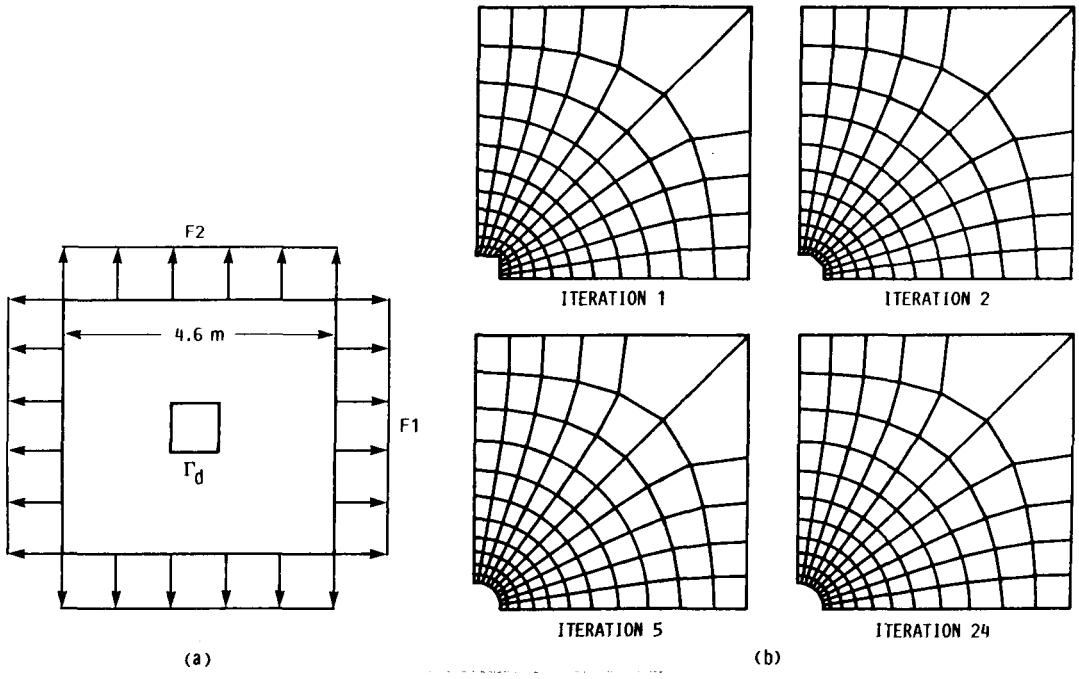

(a) Dimensions of initial input.
(b) Variation of shape during iterative procedure.

Figure 7.—Shape optimal design of hole in square sheet. Plane stress; finite elements, 110; design variables, 11; objective function, Von Mises equivalent stress; area of hole, 0.64 m^2. Only one-fourth of the sheet is modeled.

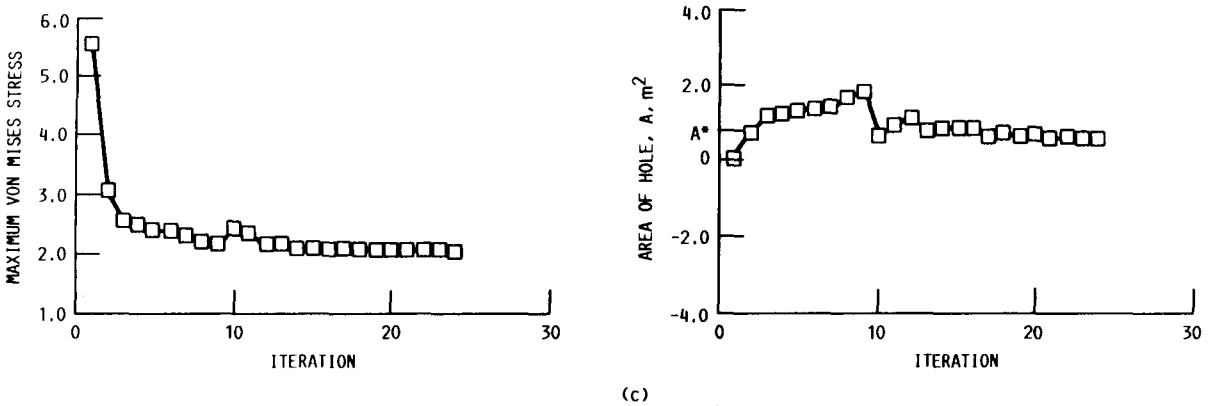

(c) Convergence history of iterative procedure. Area of hole, A, 0.64 m^2.*
Figure 7.—Continued.

For the applied symmetrical loading, the initial square hole converged to a circular hole as expected for the specified optimality criterion. The maximum Von Mises stress within the body was reduced to just over a third of its original level.

This numerical example, amongst others, demonstrated that the solution procedure converges to expected shapes in a stable manner, overcoming problems commonly encountered in shape optimization when instabilities develop in the design boundary definition.

Researchers: H. Rodriguez (University of Michigan) and B. Steinetz (NASA Lewis).

Generalized Substructuring Utilizing Mixed Modal and Physical Representations

During the last 30 years, several approximating methods of analysis based on component mode synthesis have been introduced in the field of structural dynamics. Earlier work in this field generally employed an assumed mode method, also known as Rayleigh's method. In this method, for every desired natural frequency, a mode shape of the structure is assumed. Then, by equating the maximum kinetic energy to the maximum potential energy for this system, an expression for the natural frequency can be obtained. The main disadvantage of this method is the difficulty in selecting an appropriate set of assumed mode shapes, especially in large, complex structures.

Recently, a more accurate technique was introduced—the lumped-parameter method, or what is known now as the finite element method. In this method, we discretize the stiffness and mass properties of the whole system, forming property matrices. Then, by solving the resulting eigenvalue problem, we can obtain the system frequencies and mode shapes. Though this method was direct and more feasible, especially after the development of digital computers, it required a large number of degrees of freedom to analyze complex structures. Hence, lengthy computer execution time and extensive memory were required.

To overcome this disadvantage, several methods of dynamic substructuring have been developed in the last two decades. By substructuring, the system is divided into several substructures or components. The degrees of freedom in each substructure are reduced by expressing those displacements as a truncated set of generalized coordinates defined by displacement modes.

The motivation of dynamic substructuring has been not only the economy of the computer time and memory but also the following:

(1) The various components of a structure are designed and analyzed independently.

(2) Different amounts and types of data are available for modeling each component.

(3) There are different levels of significance or importance of various components in a system, which require more or less precise modeling.

Moreover, a great reduction in effort can be achieved if the system can be divided into identical repetitive components having the same constraints and displacement modes.

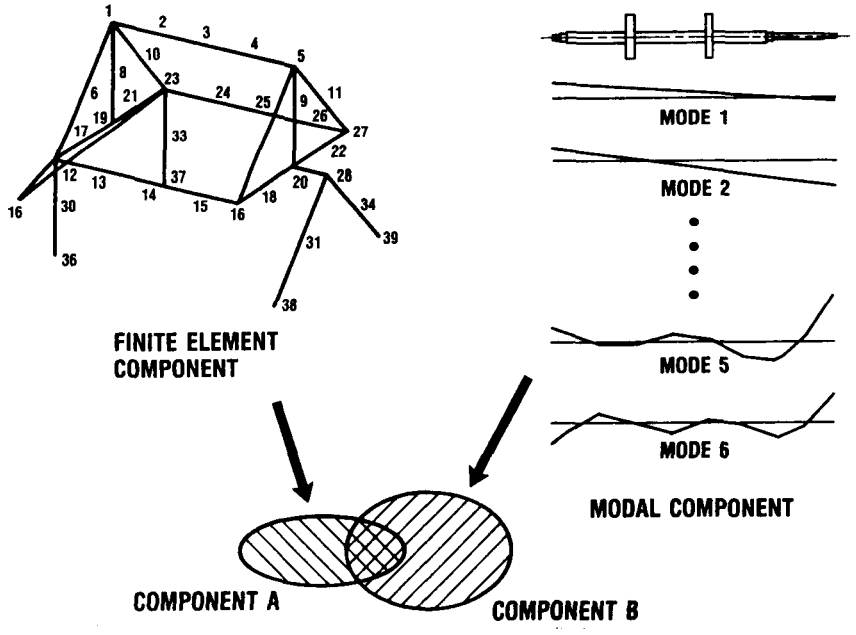

Figure 8.—Partitioning of main system into two components.

A computer program, DYSTAN 1987, has been developed to allow the assembly of a dynamic analytical model of structures, using a mixture of physical and generalized displacement coordinates. DYSTAN enables the user to use modal synthesis techniques, for parts of the system where modal data are available. While for those portions where modal data are unavailable, conventional finite element models can be used (fig. 8).

Researchers: A.A. Huckelbridge and A.A. Abdallah (Case Western Reserve) and C. Lawrence (NASA Lewis).

Characterization of Damped Structural Connections for Multicomponent Systems

Analytical models of structural systems do not normally possess characteristics which agree completely with those obtained from experiments. Although there are many possible explanations for the discrepancies, the major causes often can be attributed to inaccuracies in the data used to create the analytical model. Parameters, such as material and dimensional properties, which are usually obtained from nominal design specifications, can differ considerably from the true values, thus causing the analytical model to be inaccurate. Structural properties, such as damping and connection stiffnesses, also are extremely difficult to predetermine, yet their influence on structural response predictions is profound.

The present work investigates the feasibility of determining the characteristics of viscously damped connections from test data obtained from the complete coupled system (fig. 9). By determining the connection stiffness and damping from tests performed on the complete system, the difficulties associated with testing individual joints can be circumvented.

The component coupling portion of the procedure accommodates components which have been modeled with either finite element or modal data, obtained from analytical models or experiment. A parameter identification procedure, based on the weighted least-squares method, also is introduced. This procedure uses system test data to find an optimal set of stiffness and viscous damping connection properties. Finally, two example problems using simulated experimental data are presented. For these problems, both stiffness and damping connection properties are identified. In the first problem, a Monte-Carlo simulation is run to assess the effect of variance in the experimental data on the identified properties. In the second, the effect of friction damping is evaluated.

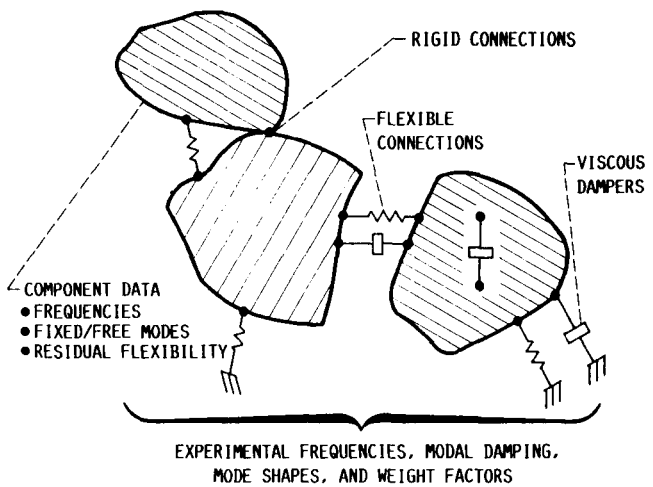

Figure 9.—System dynamics parameter identification program.

In the first sample problem, component connection properties were determined for a three-component planar beam model. From this analysis, it was found that properties could be accurately identified for a broad range of connection stiffnesses and damping by using relatively minimal measured data. The connection properties were identified by using frequency data alone. Mode shape data were not required. By performing a Monte-Carlo simulation, we determined that connection damping and stiffness could be identified even in the presence of experimental error.

In the second sample problem, equivalent viscous connection damping was identified for a model actually having friction and viscous damping. A comparison between the experimental and identified model showed that, for particular ranges of input excitation, the identified model could reliably predict peak response and settling time. However, at high levels of friction damping, the identified model did not perform as well. Since many systems include connections with nonlinearities, it is important that unrealistic predictions concerning the inservice response of the system are not made.

Researchers: C. Lawrence (NASA Lewis) and A.A. Huckelbridge (Case Western Reserve).

Microgravity Robotics Technology Program

The objective of the robotics technology program at NASA Lewis Research Center is to develop actuators, robot concepts, and control strategies which provide smooth motion, reaction minimization, and acceleration control for use in the microgravity laboratory environment.

There are two related motion control problems associated with the operation of robots in a microgravity environment. The first involves the transport of specimens without exceeding predefined microgravity acceleration limits. The second involves the transport of other objects relatively quickly while minimizing reaction forces transmitted to the robot's surroundings through attachment points. The simplest solution to both is to move the robot arm so slowly that accelerations and forces are maintained within acceptable limits. A better approach is to use mechanisms and control strategies which are inherently smooth and/or compensate for reactions. These techniques will improve robot productivity in the space laboratory.

Roller, or traction, drives provide significant benefits to robotic applications by providing smooth operation and eliminating backlash. The objective of traction-driven robot research in this program is to (1) determine the suitability of traction drives for space robot applications, (2) measure critical material and environment-related performance parameters, and (3) exploit their beneficial characteristics by developing suitable traction-driven robot joint concepts.

The design of a roller drive for a robot depends on traction performance (traction coefficient, load capacity, wear rate, fatigue life, etc.) of the selected materials and roller configurations. These in turn depend on operating conditions. A unique test rig will be used to investigate the effects of these operating conditions on material performance. This program will aid in the understanding of roller contact phenomena in nonatmospheric environments as well as provide data to design future roller-driven robot actuators.

The dynamics and control research, a cooperative effort between NASA Lewis, Case Western Reserve University, and Carnegie Mellon University has focused on the operation of a robot while limiting transmission of base reactions to the surrounding environment. Manipulators used in space applications will, in general, have kinematic redundancy to facilitate the performance of tasks. For example, redundancy will be required for obstacle avoidance and to avert singular configurations. In certain applications, the redundant degrees of freedom can also be used to minimize base reactions. In simplest terms, moving the additional sections of the manipulator in a direction inertially opposite to the movement of the end-effector minimizes the base reactions.

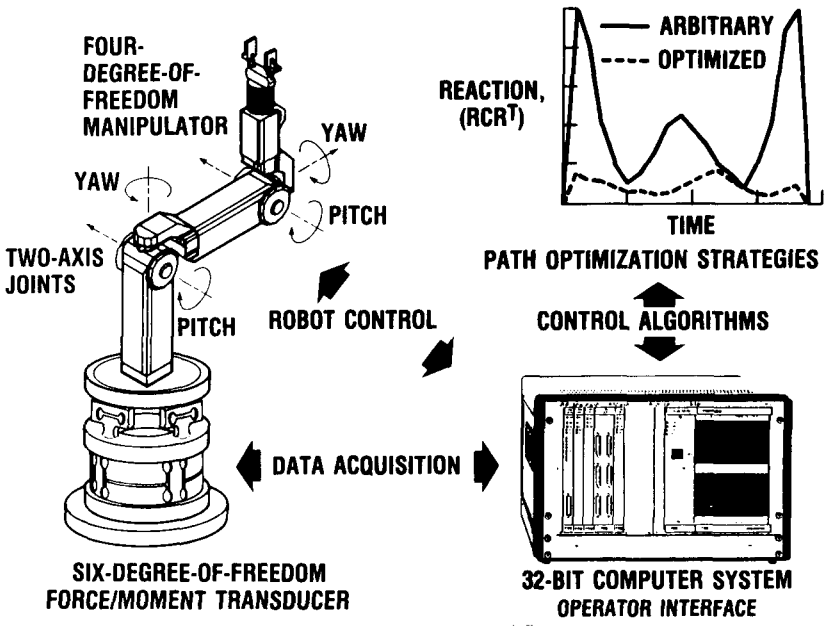

Figure 10.—Microgravity manipulation demonstration test bed.

In the procedures developed thus far, an optimization strategy identifies the joint motions that will minimize the resulting base reactions. The joint trajectory strategies were incorporated into a general computer program to simulate and control manipulators with any number of links, joints, and degrees of redundancy. By applying this code to manipulators with various degrees of redundancy, it was found that it is possible to design manipulators that will be capable of operating with minimal base reactions.

A microgravity manipulator test bed is being constructed to demonstrate the specialized control strategies and to assess the performance of roller-driven joints. The main features of this demonstrator, as shown in figure 10, are a four-degree-of-freedom traction-driven robot arm, a base reaction sensor, and a control computer. Future efforts will include evaluation of real-time feedback of reaction forces for improved base reaction compensation, measurement of end-effector acceleration and vibration, and experimental evaluation of advanced drive mechanisms.

Researchers: D.A. Rohn and C. Lawrence (NASA Lewis) and A.S. Brush (Sverdrup).

Base Reaction Optimization of Redundant Manipulators for Space Applications

One of the problems associated with manipulators that have been proposed for space applications is that the reactions transmitted to the base of the manipulator as a result of the motion of the manipulator cause undesirable effects on the dynamic behavior of the supporting space structure. It is therefore necessary to minimize the magnitude of the forces and moments transmitted to the base. In the present research we show that kinematic redundancy can be used to minimize the magnitude of the base reactions.

Manipulators used in space are operated under microgravity conditions. Furthermore, such manipulators will probably have redundant degrees of freedom in order to facilitate the performance of tasks. (It is well known that redundant manipulators can be used to avoid obstacles and avoid singular configurations.) In this research, we are concerned with planning trajectories for redundant manipulators operating under microgravity conditions in space.

The forces and moments transmitted by such manipulators to the supporting structure will, in general, act as a disturbance to the spacecraft and therefore have an undesirable effect on the dynamic behavior of the spacecraft. Compensating for the disturbance by means of a suitable control scheme is extremely difficult and expensive. An alternative approach, described in this research, is to plan a trajectory which minimizes the magnitude of the forces and moments transmitted by the manipulator to the supporting structure. In particular, we develop and apply a methodology for using kinematic redundancy to minimize the magnitude of the base reactions generated by the motion of the manipulator.

The manipulator trajectory-planning problem reduces to solving the inverse-kinematic problem for the joint variables given to the trajectory in the task-space. In the case of a nonredundant manipulator, this inverse-kinematic problem has a unique solution; whereas, in the redundant case, there are an infinite number of solutions to the inverse-kinematic problem. In this research, we pose an optimization problem of minimizing the base reactions in order to obtain a unique solution to the inverse-kinematic problem.

For a redundant manipulator, the number of degrees of freedom is greater than the minimum number of degrees of freedom required to perform a task.

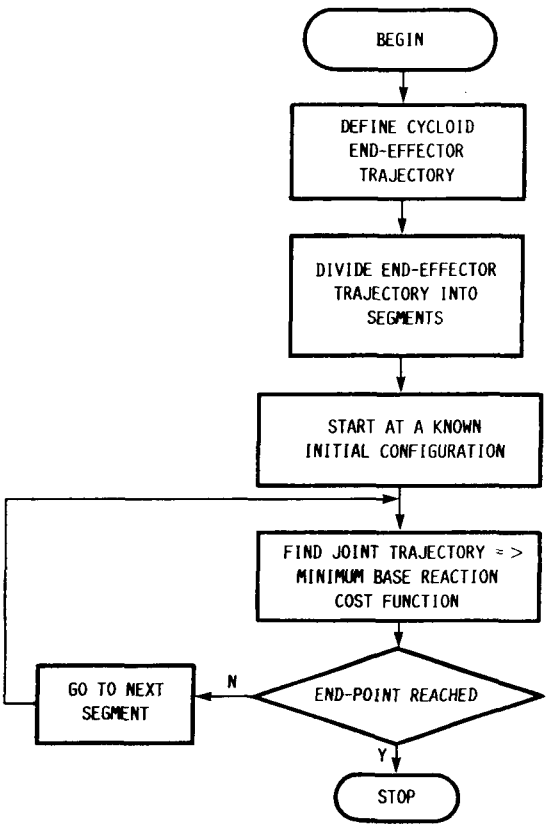

Figure 11.—Algorithm of trajectory planning.

Therefore, there are an infinite number of joint-space solutions for a specified end-effector position. From these solutions, we can select a joint-space solution based on certain criteria. In this paper, we use the minimization of the base reactions as the criterion to select the appropriate joint-space solution.

The trajectory-planning problem is split into two parts, enabling us to deal with the end-effector trajectory and joint trajectories separately. The first part is the generation of an end-effector trajectory that will satisfy certain motion constraints. The motion constraints of interest are the maximum acceleration of the end-effector trajectory and the total time of the task. The second part poses the inverse-kinematics problem for determining the joint trajectories as an optimization problem with a cost function that is a measure of the base reactions. A computer program written in Pascal has been developed to implement the methodology. The flowchart in figure 11 illustrates the basic

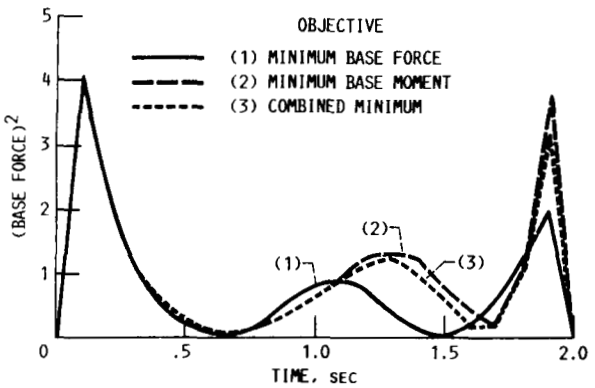

Figure 12.—Optimized magnitude of base force.

algorithm. The algorithm was applied to a four-degree-of-freedom spatial manipulator proposed by NASA Lewis.

From the results obtained (fig. 12), we observe that the cost function that weighs both the base force and base moment is most suitable for minimizing the base reactions.

Researchers: C.L. Chung and S. Desa (Carnegie-Mellon) and C. Lawrence (NASA Lewis).

Development of Hypersonic Engine Seals

High-temperature seals are required to seal structural panel joints and interfaces of advanced variable-geometry hypersonic engines. The seals must prevent extremely hot (up to 5000 °F) high-pressure (140 psi maximum) engine flow gases, including unburned hydrogen, from escaping past the movable engine panels. Leakage of these hot flow-path gases could cause severe damage of the engine panel articulation systems and catastrophic loss of the engine and vehicle. Several panel-edge seals showing promise of sealing the interfaces between the movable engine side walls and the stationary engine splitter walls were developed in this investigation.

Materials for these seals were selected for their excellent ability to operate at high (up to 2300 °F) temperatures, minimizing required coolants, and for their stability in the chemically hostile hydrogen-oxygen environment. The ceramic-wafer seal is made of stacked ceramic wafers mounted in a seal channel along the edge of the movable engine panel, as shown in figure 13(a). The seal conforms to engine wall distortions by the relative sliding of adjacent wafers. Various techniques (such as the pressurized metal bellows shown) can be used to transversely preload the ceramic wafers against the engine wall. The ceramic-wafer material, size, shape, tolerances, and loading must be optimized for the final seal application. The ceramic-wafer/ceramic-sleeve seal (fig. 13(b)) was constructed by inserting the ceramic wafers in a flexible ceramic sleeve braided of alumina-boria-silicate yarns.

The multiple-ply ceramic-sleeve seal shown in figure 13(c) is constructed of several braided ceramic sleeves tightly stretched over one another forming a

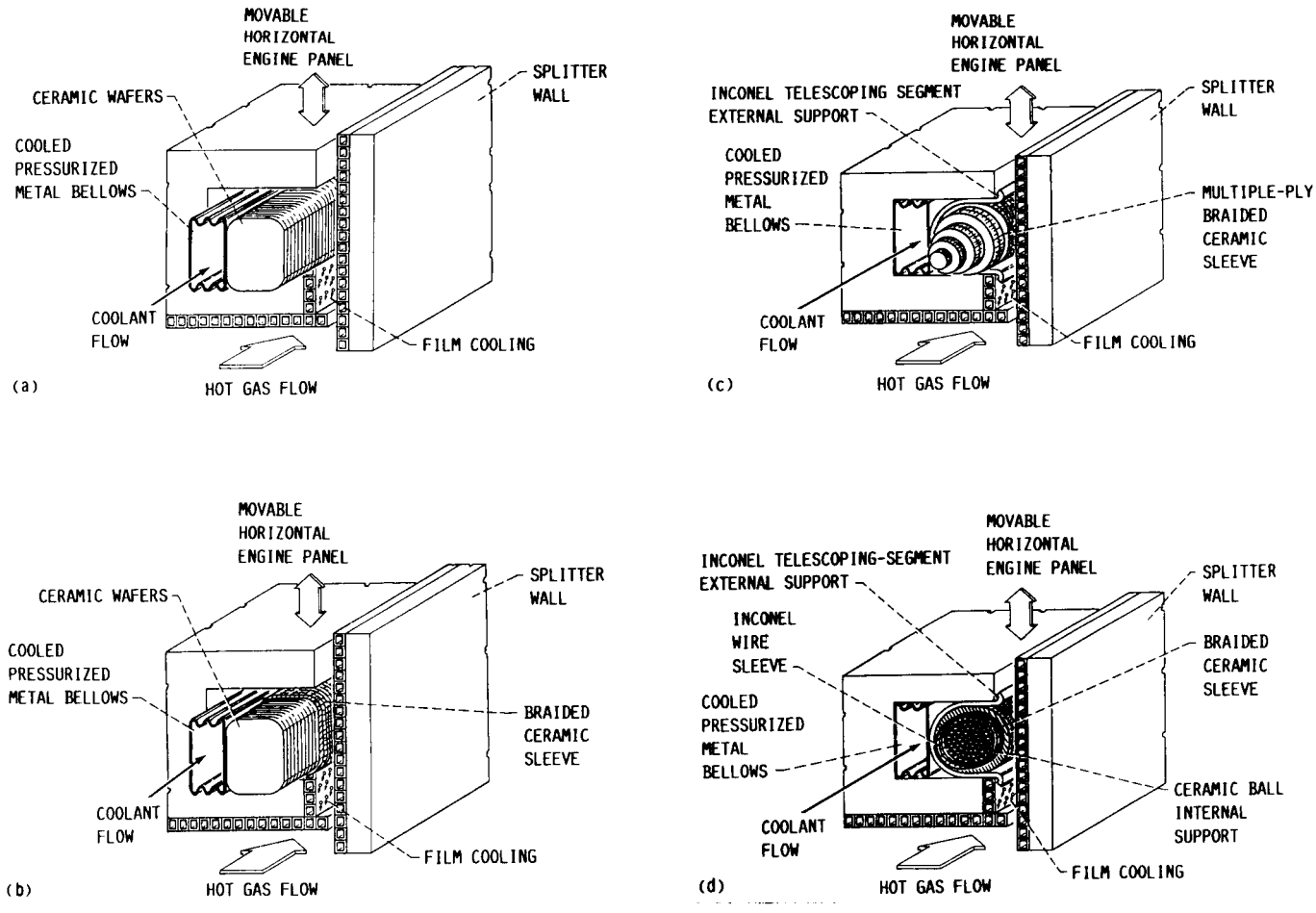

(a) Ceramic-wafer seal.
(b) Ceramic-wafer/ceramic-sleeve seal.
(c) Multiple-ply ceramic-sleeve seal.
(d) Ceramic-ball/ceramic-sleeve seal.

Figure 13.—Hypersonic engine panel-edge seal concepts.

densely-packed ceramic rope. The seal was inserted in omega-shaped telescoping sheet-metal segments (such as Inconel), fitted in the seal groove, and preloaded by the pressurized metal bellows shown.

The ceramic-ball/ceramic-sleeve seal shown in figure 13(d) consists of a braided ceramic sleeve internally packed with small ceramic balls. The ceramic balls easily roll over one another, allowing the seal to conform to both localized engine wall irregularities and global engine wall distortions.

Seal room-temperature leakage performance was ranked as a function of applied air pressure differential, seal preload, and adjacent wall condition. The results of these tests are (in order of increasing leakage) the ceramic-wafer seal; the ceramic-wafer/ceramic-sleeve seal, the multiple-ply ceramic-sleeve seal, and the ceramic-ball/ceramic-sleeve seal. Results of some of these leakage measurements are plotted in figure 14 as a function of applied pressure differential for a straight engine wall condition. All of the seals except the ceramic-ball/ceramic-sleeve seal meet the tentative maximum leakage criterion for many combinations of applied seal pressure differential and seal preload. The seals exhibit similar behavior when tested against an engine simulated wavy wall.

An analytical seal leakage model was developed for the ceramic-wafer seal relating seal leakage flow rate to gas pressure, temperature, and viscosity and to seal size, length, and apparent seal leakage gap. The model allows seal designers to estimate seal leakage flow rate for engine gas mixtures, pressures, and temperatures.

High-temperature friction and durability tests of flexible ceramic fabric, candidate seal material, were

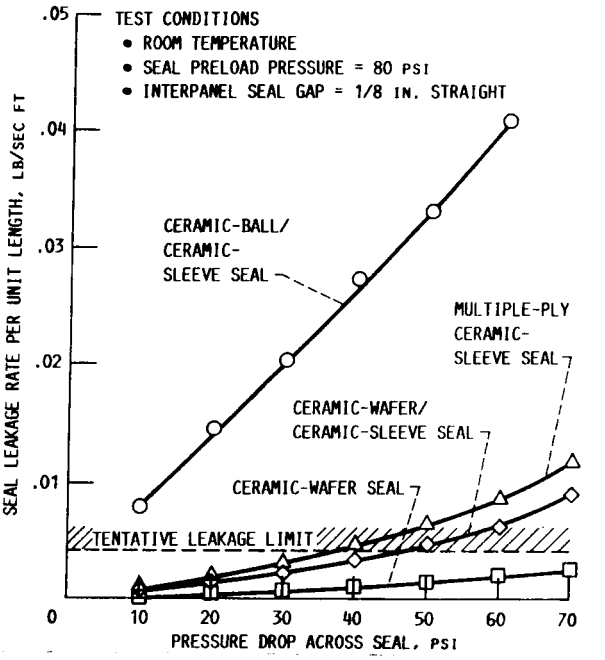

Figure 14.—Seal leakage rates as function of applied seal pressure differentials.

conducted with NASA Lewis' pin-on-disk machine. Excessive friction coefficients ($\mu > 1$) were measured when the ceramic seal fabric was slid against Inconel X–750, a candidate engine material. Application of thin solid lubricant films such as silver/calcium fluoride or gold to the alumina-boria-silicate fabric (Nextel) reduces friction coefficients by 50 percent and minimizes fabric damage when the fabric is heated from room temperature to 1560 °F.

Researchers: B. Steinetz and C. Dellacorte (NASA Lewis) and P.J. Sirocky (Sverdrup).

Experimental Investigation of Propfan Aeroelastic Response With Mistuning in Off-Axis Flow

An experiment was performed to investigate the effects of frequency and mode shape mistuning on the aeroelastic response of two propfan model rotors. Mistuning refers to the property differences that exist between the blades of a rotor. If the blades of a rotor are identical, then theoretically all the blades will have the same aeroelastic response amplitudes. The experiment showed that both inherent mistuning and intentional alternate mistuning had a significant effect on the response of the blade vibratory amplitudes. Therefore, mistuning should be included in propfan aeroelastic response analyses for reliable blade design.

Two propfan research models, the SR3C–X2 and the SR3C–3, (hereafter referred to as –X2 and –3, respectively), were used for the experiment. The models had the same geometry (each 2 ft in diameter) and material, but differed in natural frequencies and mode shapes. These differences were designed into the blades by varying the ply orientations of the laminated composite blade material.

Blade vibratory strain amplitudes were compared for the three rotor configurations shown in figure 15. One rotor had all –X2 blades, another had all –3 blades, and a third had both –X2 and –3 blades arranged in an alternate pattern. The –X2 and –3 uniform rotors had inherent mistuning from manufacturing differences of the blades, and the mixed rotor was intentionally mistuned. The vibratory blade excitation was obtained by tilting the rotor shaft in the free stream to obtain off-axis flow into the rotor. This resulted in a dominant excitation and blade response at a frequency of once-per-revolution, referred to as *1P*.

Figure 16 shows a typical variation of the *1P* vibratory strain amplitudes of the blades in the uniform and mixed rotors as a function of rotational speed. The data show that the *1P* strain amplitudes of the uniform –X2 rotor are much larger in magnitude and variation than those of the uniform –3 rotor. However, in the mixed rotor the amplitudes of the –X2 blades drop significantly and are below those of the –3 blades, but the –3 blades have relatively small changes in amplitude compared to the blades of the uniform –3 rotor. So, the intentional alternate mistuning was beneficial since it caused a large reduction in the *1P* amplitudes of the higher responding –X2 blades, but a relatively small change in the *1P* amplitudes of the lower responding –3 blades. It is interesting to note

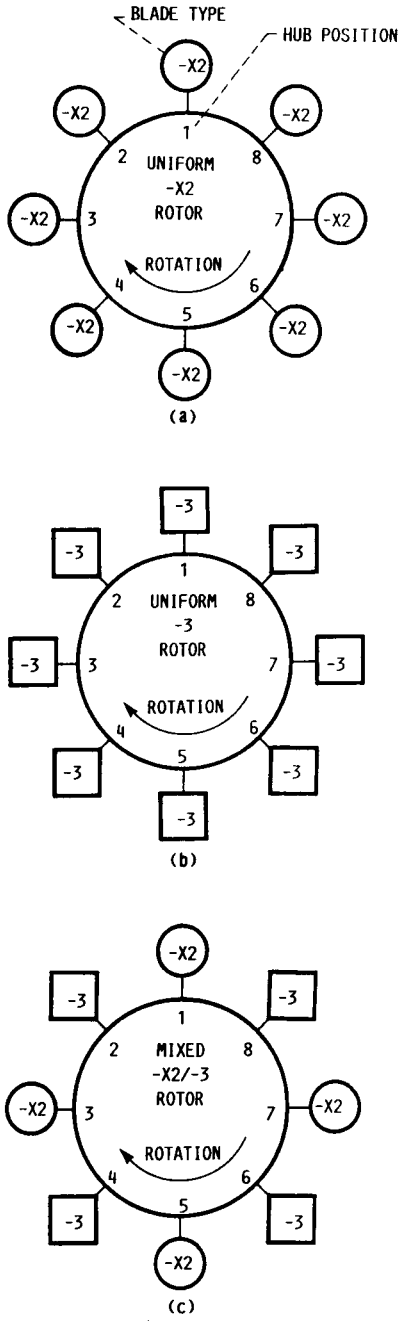

(a) Uniform SR3C–X2 rotor.
(b) Uniform SR3C–3 rotor.
(c) Mixed SR3C–X2/SR3C–3 rotor.

Figure 15.—Uniform and mixed rotor configurations. Views looking downstream.

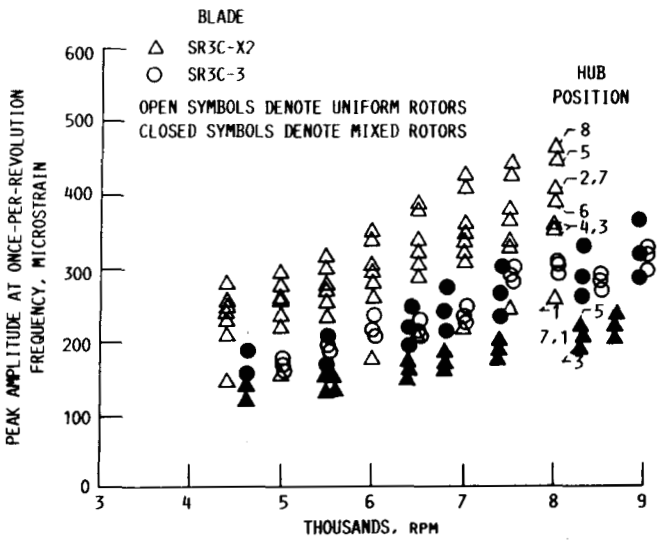

Figure 16.—1P amplitude for blades in uniform and mixed rotors. Tilt, 8°, blade angle, 48°, and strain gage, 1.

that if only a few blades in the –X2 rotor had been monitored, the maximum responding blades may have been missed; also, the order of variation of –X2 blade amplitudes could not have been predicted intuitively.

Researchers: O. Mehmed (NASA Lewis) and D.V. Murthy (University of Toledo).

Aeroelastic Response of Metallic and Composite Propfan Models in Yawed Flow

A theoretical aeroelastic response model and associated computer code (ASTROP3) were developed for predicting propfan or turborotor blade stresses or strains. (The acronym ASTROP3 stands for "aeroelastic stability and response of propulsion systems.") The model is based on normal modes of the rotating blade and three-dimensional unsteady compressible, lifting-surface aerodynamic theory including both aerodynamic and structural mistuning for blades.

The code was validated by applying it to five wind-tunnel propfan research models that were tested at NASA Lewis Research Center for aeroelastic response due to yawed flow. These models include SR–5, SR–3, SR3C–X2, SR3C–3, and SR3C–X2/SR3C–3. The blades of the first two models were made of titanium and those of the last three models were molded from graphite-ply/epoxy-matrix laminated material. The level of mistuning in the first four models was very small and was due only to manufacturing tolerances. However, the fifth model was intentionally mistuned for a particular type of mistuning that is characterized by the differences in blade frequencies, mode shapes, steady-state deflected shape, and motion-dependent unsteady aerodynamics.

Figures 17 and 18 show the calculated and measured blade oscillatory stress amplitudes due to yawed flow of the SR–5 and SR–3 wind tunnel models, respectively. The variation of the calculated stress around a strain gage is illustrated by a vertical bar in these figures. The relative flow Mach number (or helical Mach number) at the blade tip for both the models is high subsonic. The correlation between theory and experiment is good for both models. A similar correlation was observed for the other three models.

After validating the code, additional parametric blade stress calculations were performed to investigate the effects of (1) the number of modes used for each blade in the modal analysis method, (2) the blade flexibility, (3) the type and level of blade mistuning, and (4) the number of propfan blades. These calculated results, although not shown herein, led to several new and interesting conclusions:

(1) Blade stresses are sensitive to the blade frequency and mode shape mistuning. A ±5-percent alternate frequency mistuning does not have a significant influence on blade stresses for the metallic blade (SR–5). But both frequency and mode shape mistuning

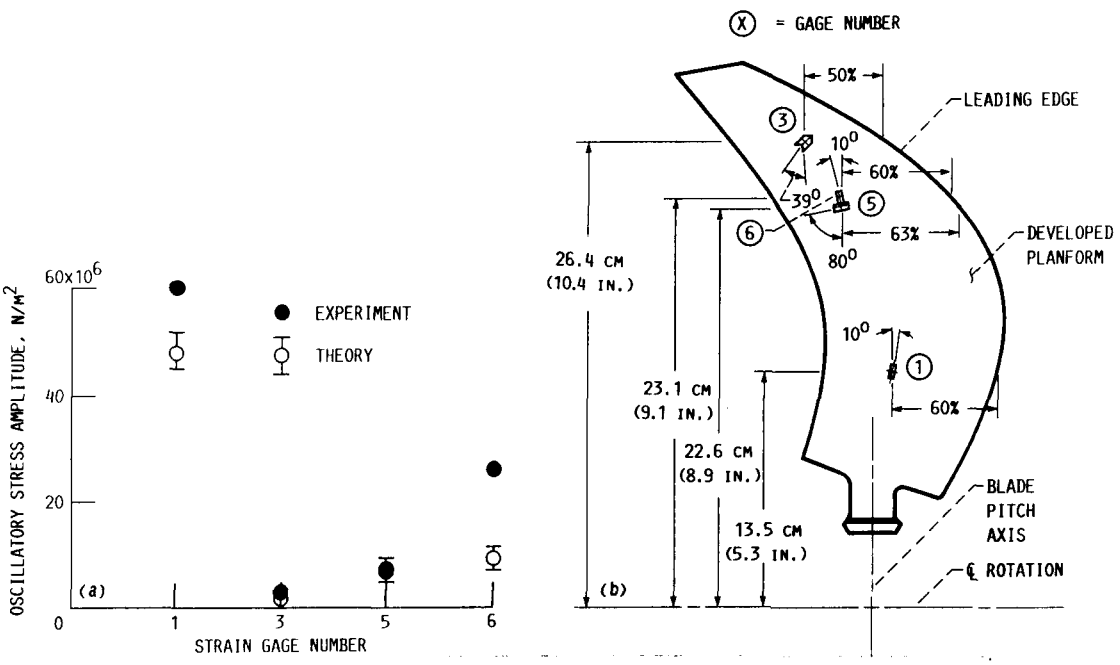

(a) Oscillatory stress amplitude as function of strain gage number.
(b) SR–5 strain gage locations on suction side.

Figure 17.—Comparison of calculated and measured blade stresses. SR–5 model test point number 8511.

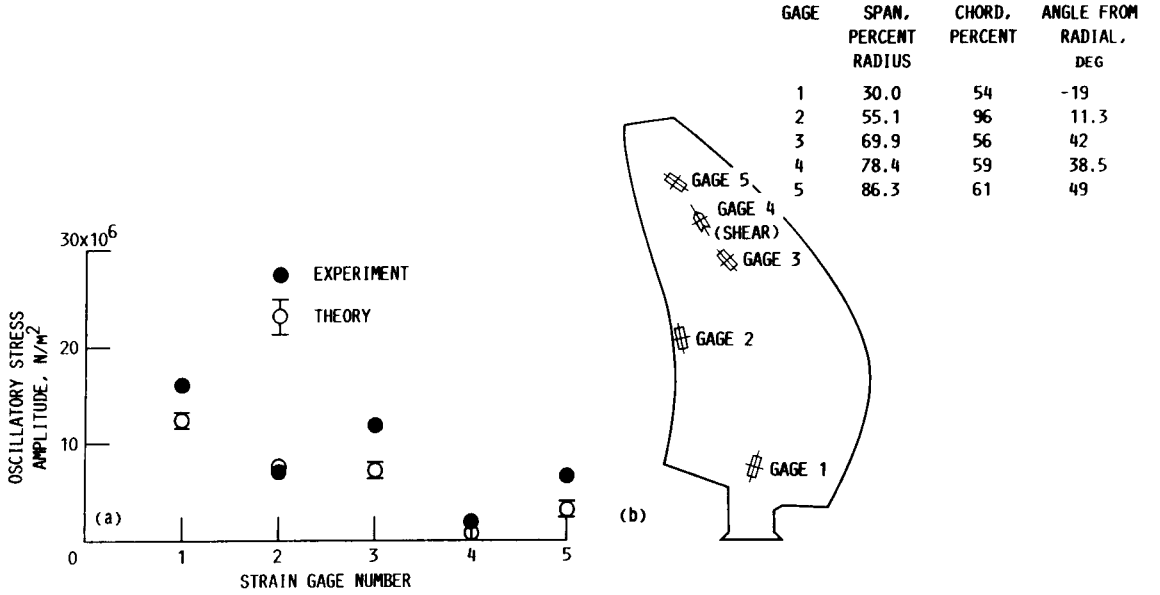

GAGE	SPAN, PERCENT RADIUS	CHORD, PERCENT	ANGLE FROM RADIAL, DEG
1	30.0	54	-19
2	55.1	96	11.3
3	69.9	56	42
4	78.4	59	38.5
5	86.3	61	49

(a) Oscillatory stress amplitude as function of strain gage number.
(b) SR–3 strain gage locations on suction side.

Figure 18.—Comparison of calculated and measured blade stresses. SR–3 model test point number 190.

have beneficial effects on composite blade strains due to yawed flow. This conclusion, which was confirmed by experimental results, is contradictory to the common belief in the published literature that the mistuning has an adverse effect on blade strains. This finding demonstrates that the mistuning must be included in aeroelastic response analysis of turborotors.

(2) The first two blade normal modes are adequate to predict the response due to yawed flow.

(3) A decrease in blade stress amplitudes due to yawed flow occurs with an increase in number of blades.

Researchers: K.R.V. Kaza (NASA Lewis), M. Williams (Purdue University), O. Mehmed (NASA Lewis), and G.V. Narayanan (Sverdrup).

Vibration and Flutter Characteristics of the SR7L Large-Scale Propfan

An investigation of the vibration characteristics and aeroelastic stability of the SR7L Large-Scale Advanced Propfan has been performed using a finite element blade model and an improved aeroelasticity code. Analyses were conducted for different blade pitch angles, blade support conditions, number of blades, rotational speeds, and free-stream Mach numbers.

A finite element model of the blade was used to determine the blade's vibration behavior and sensitivity to support stiffness. The calculated frequencies and mode shapes obtained with this model agreed well with the published experimental data. Parametric studies involving the blade support stiffness values showed that the bending torsional frequencies were generally insensitive to the support stiffness used. However, the blade edgewise frequencies were particularly sensitive to the out-of-plane support stiffness used (fig. 19).

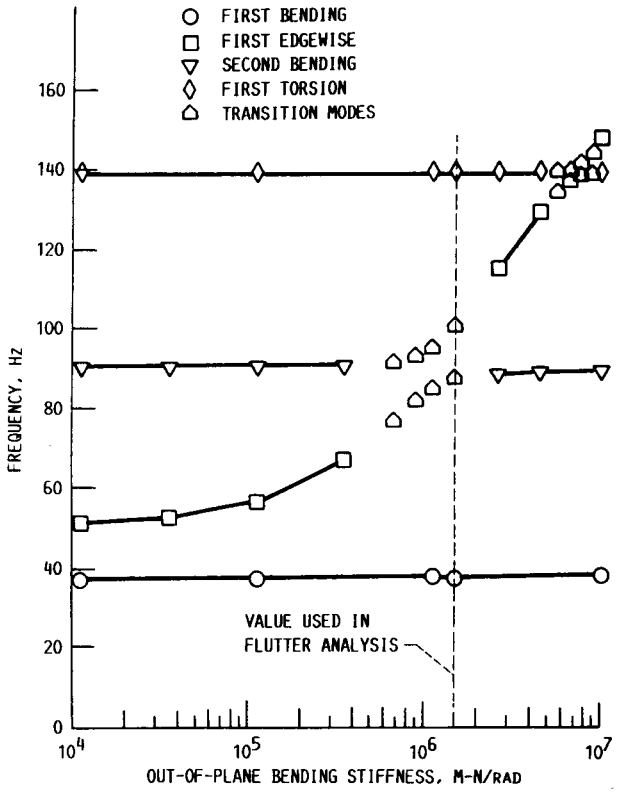

Figure 19.—SR7L frequencies as function of out-of-plane bending stiffness.

A computer code recently developed at NASA Lewis Research Center and based on three-dimensional, subsonic, unsteady, lifting surface aerodynamic theory was used for the aeroelastic analysis to examine the blade's stability at a cruise condition of Mach 0.8 at 1700 rpm. The results showed that the blade is stable for that operating point. However, a flutter condition was predicted if the cruise Mach number was increased to 0.9 (fig. 20).

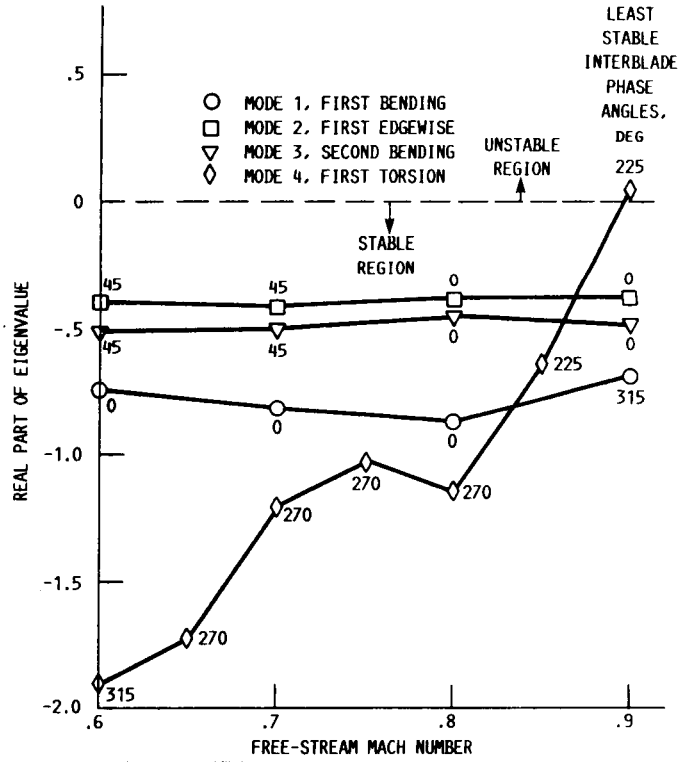

Figure 20.—SR7L damping as function of Mach number for original support.

Researchers: R. August (Sverdrup) and K.R.V. Kaza (NASA Lewis).

Vibration, Performance, Flutter, and Forced Response Characteristics of a Large-Scale Propfan and Its Aeroelastic Model

An investigation of the vibration, performance, flutter, and forced response of the large-scale propfan, SR7L, and its aeroelastic model, SR7A, has been performed by applying available structural and aeroelastic analytical codes and then correlating the measured and calculated results. The objectives of this investigation were (1) to continue to validate new advanced propfan analysis methods and (2) to assess the SR7A and SR7L dynamic simulation. Finite element models of the blades were used to obtain modal frequencies, displacements, stresses, and strains. These values were then used in conjunction with a three-dimensional, unsteady, lifting surface aerodynamic theory for the subsequent aeroelastic analyses of the blades.

The agreement between measured and calculated frequencies and mode shapes for both models is very good. Scaling the natural frequencies by multiplying the frequencies by blade tip radius shows that the SR7A blade matches the dynamic characteristics of the SR7L blade very well (fig. 21). Calculated power coefficients correlate well with those measured for low advance ratios. Flutter results show that both propfans are stable at their respective design points (fig. 22). There is good agreement between calculated and measured blade vibratory strains due to excitation resulting from yawed flow for the SR7A propfan.

In general, the aeroelastic results further demonstrate the validity of the ASTROP code, but also point out the need for more improvement in the forced response analysis. The similarity of structural and aeroelastic results also show that the SR7A propfan properly simulates the SR7L characteristics.

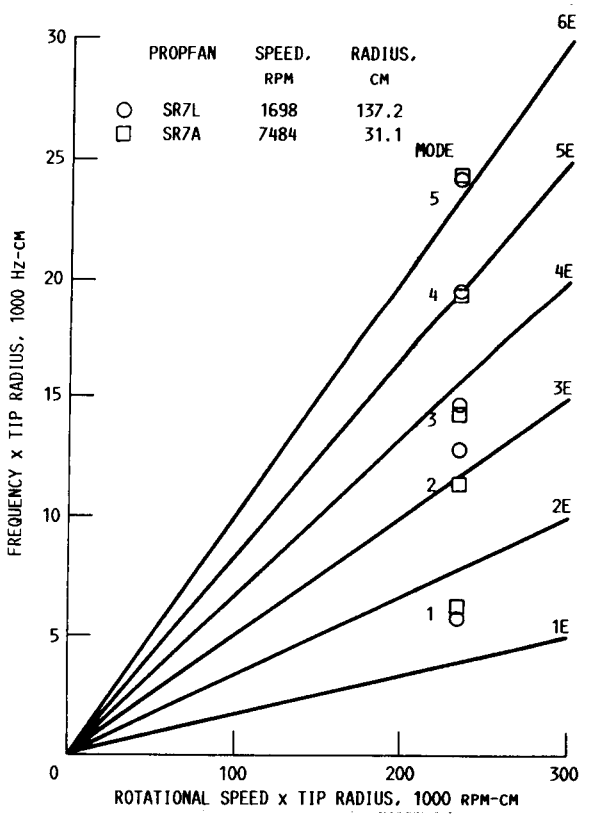

Figure 21.—SR7A, SR7L modified Campbell diagram.

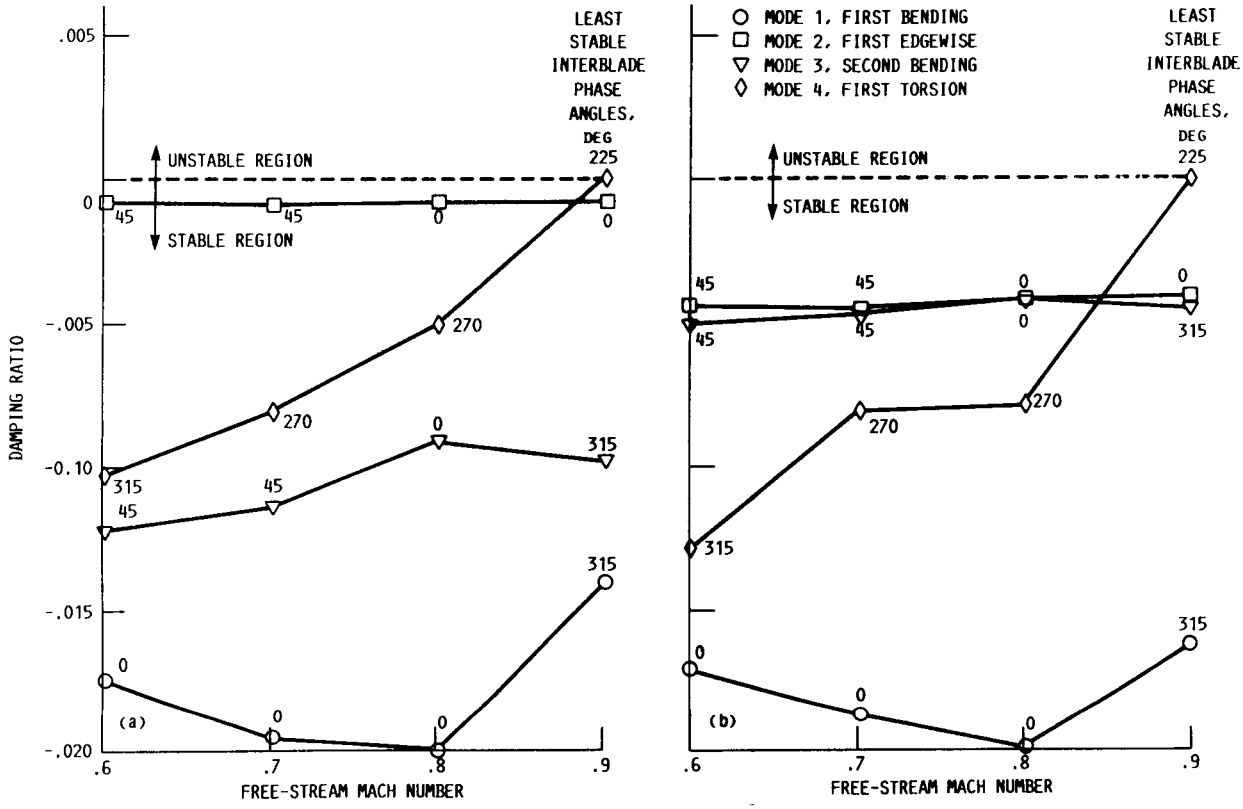

(a) SR7A.
(b) SR7L.

Figure 22.—Calculated modal damping.

Researchers: R. August (Sverdrup) and K.R.V. Kaza (NASA Lewis).

Application of a Semianalytical Technique for Sensitivity Analysis of Unsteady Aerodynamic Computations

The computation of derivatives of response quantities to design parameters, known as sensitivity analysis, plays an important role in developing reliable and efficient procedures for design optimization of practical aerospace structures. For aeroelastic problems, the sensitivity derivatives can also be useful in computational schemes for aeroelastic analysis and in computing the derivatives of the flutter Mach number and flutter frequency.

These sensitivity derivatives can be calculated using a straightforward finite-difference approach. However, experience in other engineering disciplines suggests that a semianalytical approach may prove to be more computationally efficient. This paper presents a semianalytical sensitivity analysis of the subsonic unsteady aerodynamics used in flutter analysis, so that the derivatives of the generalized unsteady aerodynamic forces can be computed. As a first step, only non-shape-dependent variables representing the flow conditions and the structural motion are considered.

The semianalytical approach to the sensitivity analysis of a response function consists of an analytical differentiation of the original function with respect to an intermediate function and the evaluation of this derivative by numerical differentiation. The semianalytical approach combines the efficiency of the analytical approach with the ease of implementation of the finite-difference approach.

Using the semianalytical approach, we show that the sensitivity of the generalized aerodynamic force is equal to the generalized force acting on the blade resulting from a "pseudo-pressure differential" across the blade surface. The pseudo-pressure differential is shown to be equal to the pressure distribution that gives rise to a "pseudo-upwash" distribution.

The semianalytical approach is applied to two unsteady aerodynamic models: (1) an isolated airfoil in two-dimensional flow and (2) rotating propfan blades in three-dimensional flow.

Consider the generalized force (GF) on the SR3C–X2 propfan blade in the first normal mode due to motion in the first normal mode. Figure 23 shows the computed sensitivities of the generalized force with respect to the vibration frequency. The generalized force also is shown on the right vertical axis. The sensitivities calculated by the finite-difference and the semianalytical approaches are in reasonable agreement.

Figure 24 shows the percentage saving of CPU time achieved by the semianalytical approach as a function

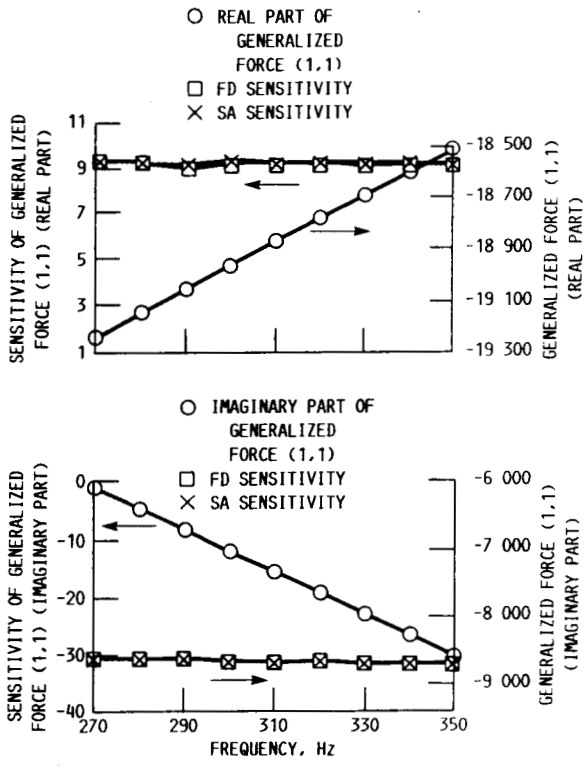

Figure 23.—Sensitivity of generalized force with respect to vibration frequency.

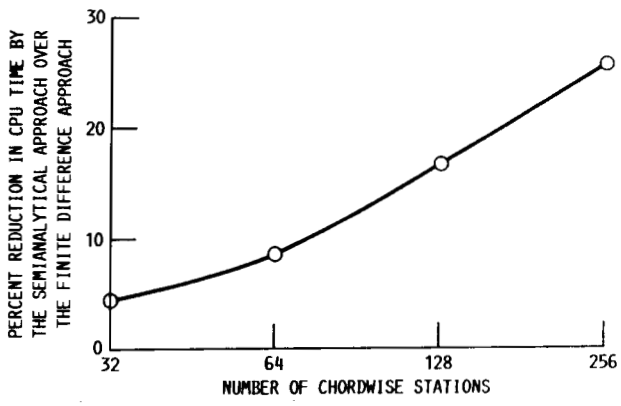

Figure 24.—Saving of CPU time as function of number of chordwise stations.

of the number of chordwise stations. The efficiency of the semianalytical approach relative to the finite-difference approach increases rapidly with the number of chordwise stations. This saving in CPU time can be significant in aeroelastic optimization of propfan blades with three-dimensional unsteady cascade aerodynamics that employ mistuning and a large number of panels.

Researchers: D.V. Murthy (University of Toledo) and K.R.V. Kaza (NASA Lewis).

Effects of Rotational Flow, Viscosity, Thickness, and Shape on Transonic Flutter Dip Phenomenon

The transonic flutter dip phenomenon associated with blade sweep on thin airfoils for propfan blades is investigated by using an integrated two-dimensional Euler/Navier-Stokes code and a two-degree-of-freedom, typical section structural model. The Euler/Navier-Stokes code solves the unsteady, two-dimensional, Reynold's averaged, compressible, full Navier-Stokes equations on a body-fitted coordinate system in a strong conservation form by using an alternating direction implicit procedure. An algebraic eddy viscosity model is included to analyze turbulent flows.

Figure 25 shows the flutter boundary for the NACA 64A010 airfoil. The boundary is obtained with the Euler version of the code by using two dissipation models. The two dissipation models, model I based on the local pressure gradient scaled by a common factor and model II based on the local pressure gradient scaled by a spectral radius, predicted the same flutter boundary except in the recovery region for the case studied. The dissipation model I predicts a flutter boundary that folds over to provide upper boundaries. No such folding over of the boundary is observed when dissipation model II is used. This indicates that the recovery portion of the flutter boundary is dependent on the dissipation model used, even though the minima of the dip is unaffected by the models.

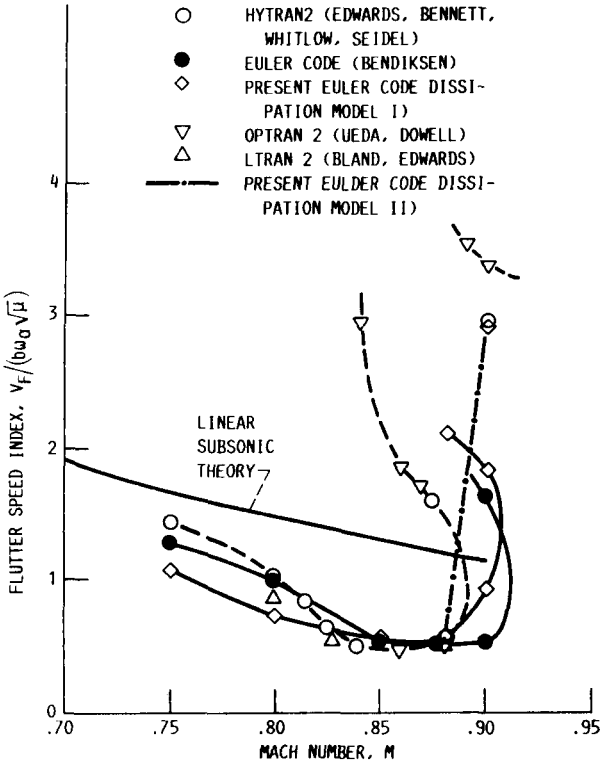

Figure 25.—Flutter boundaries for NACA 64A010 airfoil.

Figure 25 also shows a comparison of the flutter boundary obtained by using the Euler version of the code and using the dissipation model I, with published results. The published results have been obtained by an Euler code, three transonic small disturbance (TSD) codes, and a linear subsonic theory (LST) code. All the codes, except the LST code, show qualitatively the same flutter boundary. The LST code, as expected, predicts a linear drop in the flutter speed as the Mach number increases.

For Mach numbers between 0.7 and 0.82, the flutter speeds predicted by the present Euler code are less than those predicted by the TSD codes. However, for Mach numbers between 0.82 and 0.87 the flutter speeds are in good agreement. This behavior can be explained by inspecting the shock location on the airfoil. For example, for a Mach number of 0.8, the shock is near the midchord, indicating that the flow is rotational over a reasonably large area. The TSD theories are unable to model the effect of rotational flow downstream of the shock and predict a higher flutter boundary than that predicted by the present code. As the Mach number increases, the shock travels towards the trailing edge and the strength of the shock increases. For Mach numbers between 0.85 and 0.88, the shock is near the trailing edge, thereby reducing the area over which the flow is rotational. Therefore the Euler code shows the same accuracy as the TSD codes. Beyond Mach 0.88, the shock strength is sufficiently high to induce separation. The Euler and TSD codes fail to model separated flow behind shocks, and they predict qualitatively the same flutter boundary beyond Mach 0.88.

Studies, not presented here, showed that the effects of mean angle of attack, initial conditions, and viscosity on the flutter boundary are negligible on the minima of the dip but have a significant effect away from the dip.

Figure 26 shows the effect of shape and thickness on the flutter boundary calculated by using the present Euler code with dissipation model I. Also included in the figure, for comparison, is the flutter boundary calculated by using the linear subsonic theory. Four

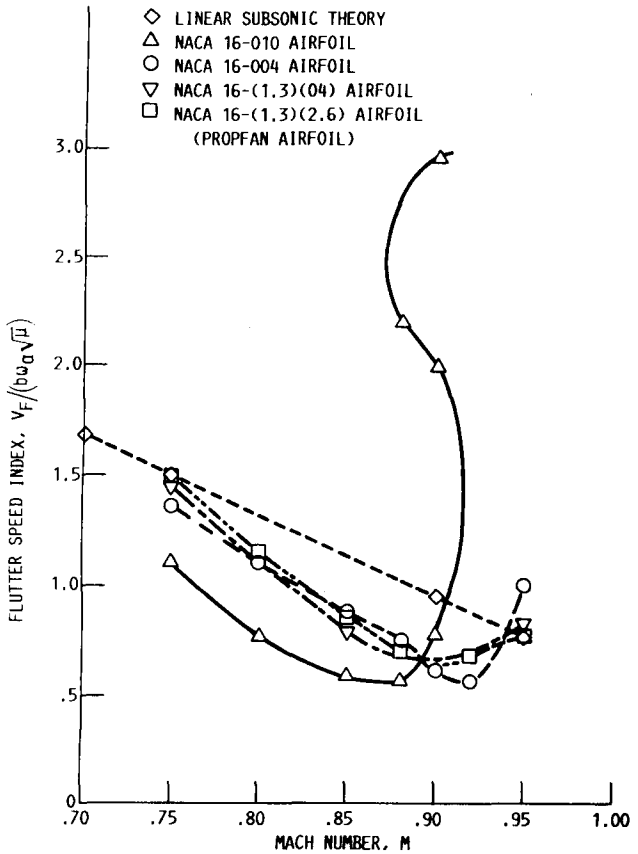

Figure 26.—Flutter boundaries for four airfoils.

NACA 16 series airfoils, 16–010, 16–004, 16–(1.3)(04), and 16–(1.3)(2.6), were considered for the study. The NACA 16–(1.3)(2.6) airfoil represents a typical propfan airfoil.

Comparison of the results for the four airfoils shows that (1) for symmetric airfoils, the transonic dip moves towards higher Mach numbers as thickness to chord ratio decreases; (2) for the thin cambered airfoil studied here, the camber effects are nullified by the effects due to reduction in thickness, and the flutter boundary is similar to a thick symmetric airfoil of the same series; and (3) the flutter characteristics strongly depend on the

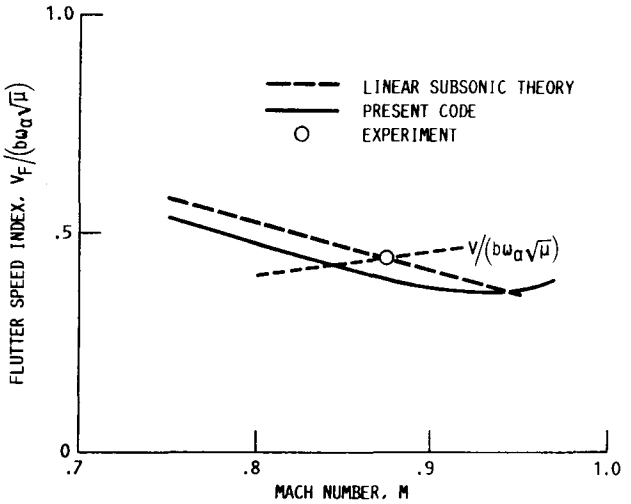

Figure 27.—Flutter boundary for SR–5 propfan simulated typical section model.

shock location and shock strength. The results presented in figure 26 show that the transonic dip is present even for thin airfoils, even though the minima of the dip is smaller than that for thick airfoils.

Figure 27 shows the flutter boundary obtained using the present Euler code with the SR–5 swept propfan simulated typical section model. The flutter boundary obtained with the LST code is also shown in figure 27 along with the velocity index curve ($V/(b\omega_\alpha\sqrt{\mu})$ versus Mach number) for this typical blade. Here V is the velocity, b is the semichord, ω_α is the torsional frequency, and μ is the mass ratio. The present Euler code gives a flutter Mach number of 0.845. This value is about 4.5 percent less than that obtained from the SR–5 propfan experiment, which may be due to the limitation of the typical structural dynamic model employed to simulate the SR–5 propfan.

Researchers: T.S.R. Reddy (University of Toledo), R. Srivastava (Georgia Tech), and K.R.V. Kaza (NASA Lewis).

Unsteady Supersonic Axial Flow Aerodynamics

A research project to design, build, and conduct experiments on a single-stage supersonic throughflow fan is now underway at the NASA Lewis Research Center. During the design stage, the question of aeroelastic stability arose. Since the aeroelastic stability was a concern, an analytical capability was needed to perform the aeroelastic stability analysis. Consequently, a computer code was developed to predict the unsteady aerodynamic loading for supersonic axial flow. This code was then incorporated into an existing aeroelastic stability code (MISER2) to perform the analysis.

In this code, Lane's equations are used to calculate the unsteady aerodynamic loads. These equations are the result of an extension of a Laplace transform method first proposed by Miles for a single airfoil with wind tunnel wall interference. Lane's formulation considers a two-dimensional cascade with a supersonic leading-edge locus having arbitrary stagger angle (blade leading edges must be ahead of Mach lines) and arbitrary interblade phase angle. The effects of airfoil thickness, camber, and steady-state angle of attack are neglected.

The NASA Lewis blade is much higher in solidity and lower in stagger angle than typical fan stages. However, the airfoil cross section is similar to that of conventional fan blades. The first mode is primarily bending and the second mode is primarily torsion. The physical properties of the 73.3 percent span location were chosen as being representative and were used in the flutter analysis (fig. 28).

Along with the results for supersonic axial flow, some comparative results were obtained for subsonic axial flow using other theories (Rao and Jones, Adamczyk and Goldstein). For supersonic Mach numbers less than 1.6, the critical reduced velocity starts at a very low value of approximately 0.5 and increases with Mach number to approximately 1.0. For relative Mach numbers greater than 1.6, the critical value is always near 1.0. The aeroelastic stability analysis predicted the blades would be unstable at supersonic relative velocities. As a result, the rotor blades were redesigned by reducing the aspect ratio, to bring the throughflow fan into the stable operating range.

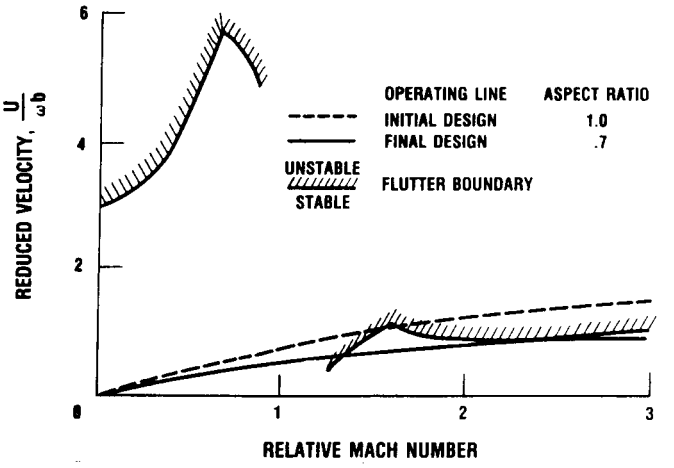

Figure 28.—Aeroelastic analysis of supersonic throughflow fan torsional flutter.

Researchers: J.K. Ramsey and R.E. Kielb (NASA Lewis).

Visual Method for Finding Complex Roots of Polynomials by Using Transputers

The extraction of roots (eigenvalues) from polynomial (characteristic) equations is often inexact. Root-finding methods such as Newton-Raphson can completely miss one or more roots of a polynomial.

A graphical method using transputers has been developed to help identify roots in an arbitrary region of the complex plane. A quick visual identification of roots in a region of the complex plane is now possible.

The method discretizes the specified complex region so that the coordinates correspond to every pixel on the display board. For each complex coordinate, z, the polynomial, $f(z)$, is evaluated. Depending on the quadrant of $f(z)$, a color value (four possible) is assigned to the z coordinate and plotted. The root(s) of the polynomial lie at the intersection(s) of the four colors.

The results of the method for the polynomial

$$f(z) = z^4 - 2.0z^3 + 1.25z^2 - 0.25z - 0.75$$

over the complex plane from $(-2, -2j)$ to $(2, 2j)$ are shown in figure 29. Note how the approximate values for the roots of $f(z)$ can quickly be found by looking at the figure.

The parallelization of this method consists of distributing a subregion of the specified complex region to a given processor. Each processor in the network evaluates the polynomial $f(z)$ for the specified subregion. The computed coordinate and color data are then sent to a display node for drawing.

The architecture for the parallel implementation of this method will be a pipeline of transputers. This type of network is easy to implement on transputers and can easily take advantage of the overlapping of network communications with computation for high-performance concurrent analyses.

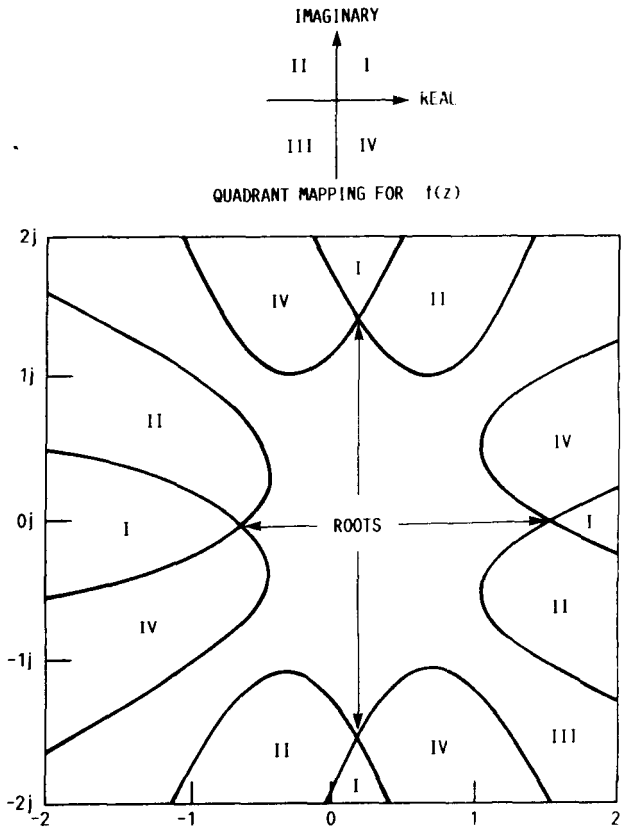

Figure 29.—Polynomial root visualization results for $f(z) = z^4 - 2z^3 + 1.25z^2 - 0.25z - 0.75$.

Researchers: G.K. Ellis (ICOMP).

Two-Dimensional Graphics Tools for a Transputer-Based Display Board

A package of two-dimensional graphics routines has been developed in an effort to standardize and simplify the user interface for a transputer-based graphics display board. The routines available take advantage of the graphics board's capabilities while presenting an intuitive approach for generating drawings. The routines allow a user to perform graphics renderings in a two-dimensional real-coordinate space without regard to the actual screen coordinates. Multiple windows, which can be placed arbitrarily on the screen, as well as the ability to use double-buffering techniques for smooth animations are also supported.

The routines are designed to be run on a transputer other than the graphics display board. The window and screen parameters are maintained locally. The conversion to device coordinates is also performed locally. The only data sent to the display board are control and device coordinate display commands.

A processor block diagram showing the world processor, the display processor, and the graphics monitor is shown in figure 30. The logical blocks showing the transformation procedures used on the two-dimensional world processor to map a drawing from world coordinates to integer device coordinates is shown in figure 31.

The routines available include rotation, translation, and scaling commands; absolute and relative point and line commands; circle, rectangle, and polygon commands; and window and viewpoint definitions commands.

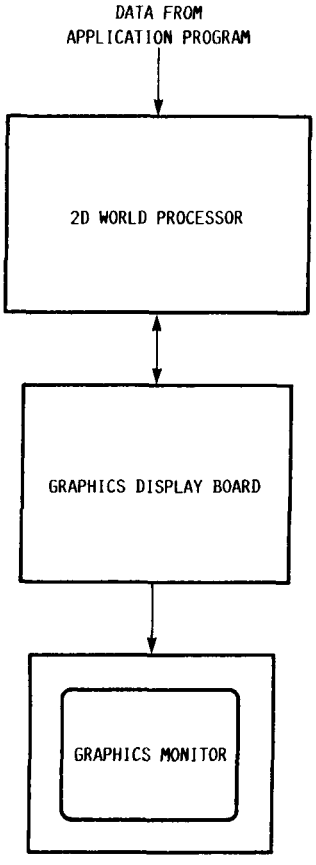

Figure 30.—Processor block diagram of transputer graphics display system.

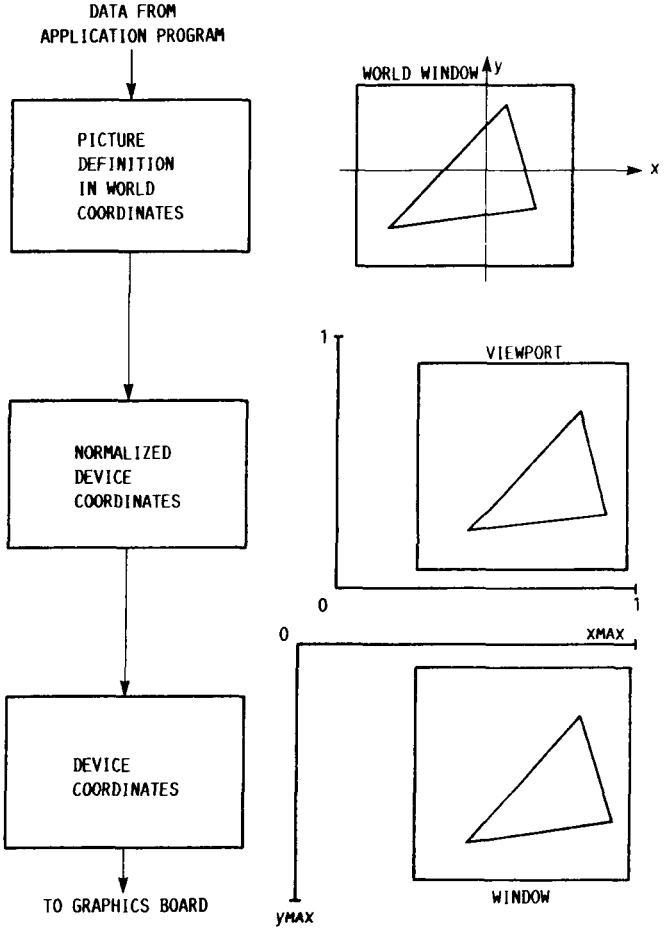

Figure 31.—Implementation of two-dimensional viewing on two-dimensional world processor.

Researchers: G.K. Ellis (ICOMP).

Distributed Computation of Graphics Primitives on a Transputer Network

A method has been developed for distributing the computation of graphics primitives on a parallel processing network. Off-the-shelf transputer boards are used to perform the graphics transformations that would normally be assigned to a single-transputer-based display processor. Each node in the network performs a single graphics primitive computation. Frequently requested tasks can be duplicated on several nodes.

The transputer network used for the computation is shown in figure 32. The buffer routines that run on each node and perform data routing through the network are shown in figure 33.

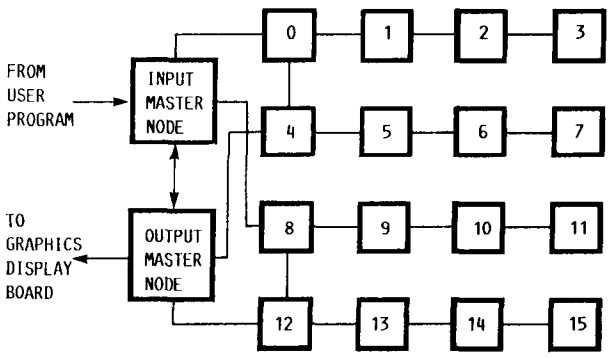

Figure 32.—Multiple processor graphics display engine showing processor.

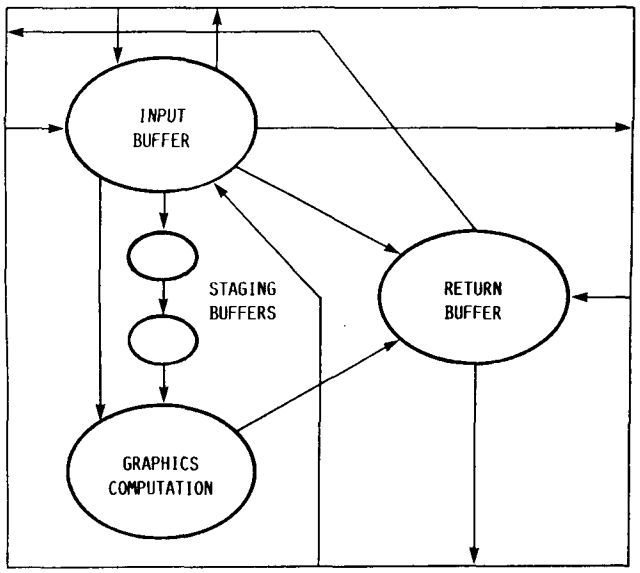

Figure 33.—Computation of node buffer processes and communication.

Results indicate that the current distribution of commands on the graphics network shows a performance degradation when compared to the graphics display board alone. A change to more computations per node for every communication (perform more complex tasks on each node) may cause the desired increase in throughput. The results for line draw and circle draw computations are shown in tables IV and V, respectively.

TABLE IV.—COMPARISON OF LINE COMPUTE–DISPLAY TIMES

Operations performed	Time, μsec
Scan convert line (0, 0) to (511, 511)	7 933
Transmit computed data to display board	12 512
Transmit data and display line	28 400
Scan convert, transmit, and display	36 399
Graphics board draw line command	14 887
Graphics board fast draw line command	3 542

TABLE V.—COMPARISON OF CIRCLE COMPUTE/DISPLAY TIMES

Operations performed, (radius = 100, center = (256, 256))	Time, μsec
Scan convert circle	2 338
Transmit computed data to display board	37 362
Transmit and display circle	54 685
Scan convert, transmit, display	57 064
Graphics board circle draw command	37 349

Researchers: G.K. Ellis (ICOMP).

Implementing Direct Spatially Isolated Problems on Transputer Networks

Parametric studies have been performed on transputer networks of up to 40 processors to determine how to implement and maximize the performance of the solution of spatially isolated problems.

The term spatially isolated refers to the class of problems that can be divided such that no data are required from any other processor for the problem solution. This, however, does not preclude the necessity of distributing and collecting initial data and final answers on the transputer network. A direct problem is one that requires a known number of iterations to be solved (i.e., not iterative).

Two types of problems were investigated in this study. A computationally intensive problem where the solution required the transmission of 160 bytes of data through the parallel network, and a communication intensive problem that required the transmission of 3 Mbytes of data through the network. This data consists of solutions being sent through the network back to the host processor, and not intermediate results for another processor to work on.

Studies were performed on both integer and floating-point transputers. The floating-point transputer features an onchip floating-point math unit and offers approximately an order of magnitude performance increase over the integer transputer on real-valued computations.

The results indicate that some minimum amount of work is required on each node per communication to achieve high network speedups (efficiencies). The floating-point processor requires approximately an order of magnitude more work per communication than the integer processor because of the floating-point unit's increased computing capability.

Figure 34 shows the results for the definite integral evaluation using the rectangle rule on a floating-point

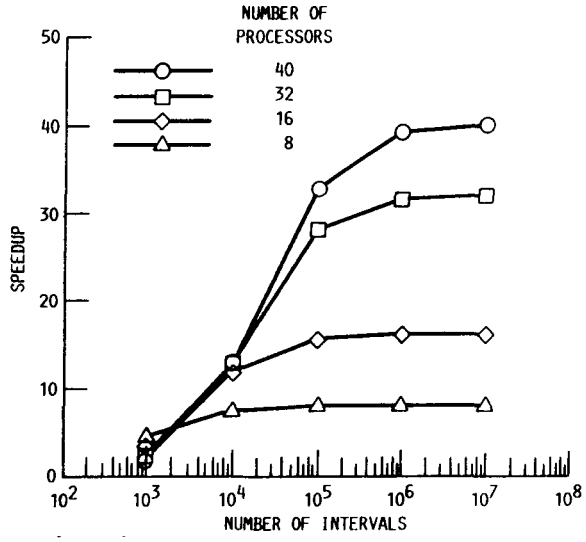

Figure 35.—Speedup of computation of definite integral on transputer network.

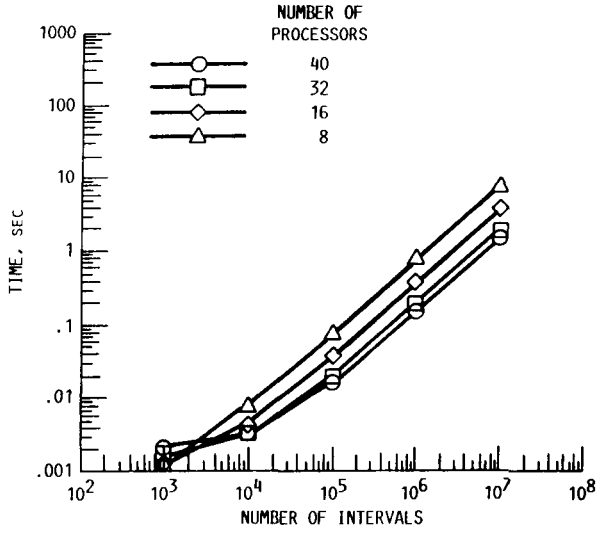

Figure 34.—Transputer network performance for solution of definite integral.

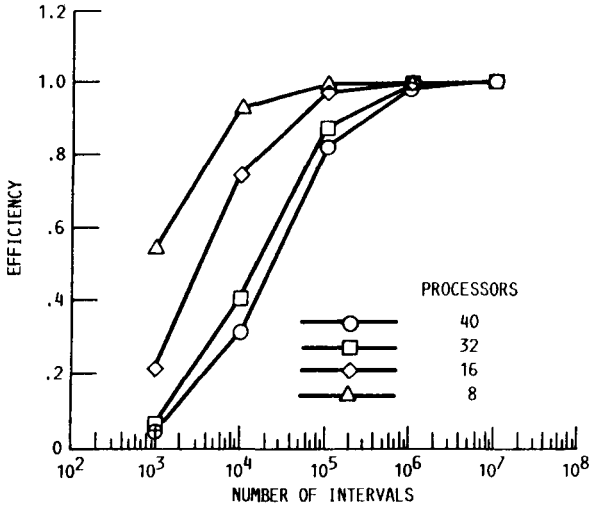

Figure 36.—Efficiency of computation of definite integral on transputer network.

processor network. The integral was evaluated on 8, 16, 32, and 40 processors. Note that for low numbers of intervals (<10,000), 8 processors perform faster than 40. This is because network communication time becomes significant when compared to computation time. Figures 35 and 36 show the same results expressed as speedup and efficiency, respectively.

Researchers: G.K. Ellis (ICOMP).

High-Speed Balancing on a Helicopter Engine

This contract effort comprised three separate tasks: (1) analysis and demonstration of high-speed balancing on a T700 power turbine module, (2) analysis of high-speed balancing on T700 gas generator modules, (3) and development of vibration diagnostics for T53, T55, and T700 engines.

Both the gas generator and the power turbine of the T700 engine operate above bending critical speeds. Close tolerances in manufacture and assembly, combined with careful low-speed balancing, allow satisfactory operation of the engine. The Army was concerned, however, that the close tolerances would be difficult to maintain through engine overhaul. Use of high-speed balancing would allow a relaxation of tolerances (thus lowering cost) and at the same time produce smoother running engines.

The T700 power turbine assembly was balanced at 20 000 rpm (its normal operating speed), applying balance corrections at three locations along the shaft axis. Results are shown in figure 37. The components of this power turbine had previously been balanced at low speed; the assembly was considered within production tolerances. The vibration was reduced considerably by high-speed balancing, both at the critical speeds and at operating speed. Analysis shows similar benefits for T700 gas generator assemblies.

To assist in repair of overhauled engines that vibrate excessively, vibration spectra were measured for operating conditions used in the acceptance test. Figure 38 shows a typical result. From left to right, vibration peaks are observed at speeds of the power turbine (*NP*), accessory gearbox, 0.89*NG* (source unknown), gas generator (*NG*), and 2*AG*. Vibration spectra of engines undergoing acceptance tests are compared with the typical spectra. If vibration at any one frequency is particularly high, this indicates a problem in the component producing that frequency. For example,

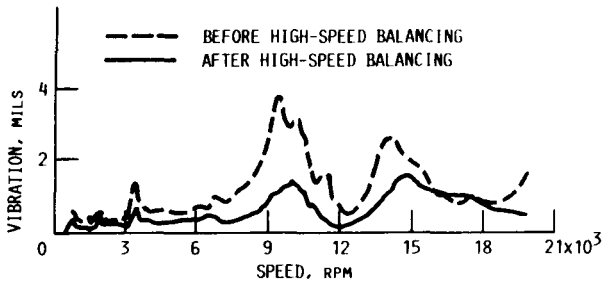

Figure 37.—T700 power turbine vibration displacement probe.

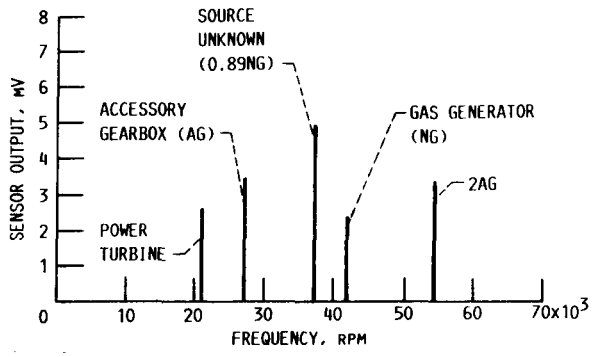

Figure 38.—T700 vibration spectrum.

high vibration at *NP* would indicate an out-of-balance power turbine. With this knowledge, only the component at fault needs to be reworked, rather than the entire engine as was previously the case. This results in considerable savings of time and resources.

Researchers: Mechanical Technology, Inc.
Technical Monitor: D.P. Fleming (NASA Lewis).

High-Load Damper Test Rig With Thrust Capability

Modern turbine engines must be designed to operate reliably, not only under normal conditions, but when abnormalities such as a lost turbine blade occur. This means that shaft dampers must sometimes tolerate higher than normal loads and amplitudes, while continuing to provide good vibration control. Damper designs other than conventional squeeze films are usually required for this. In addition, the increasing flexibility of contemporary engines and the need for seal clearance control often make it desirable to provide dampers at all bearing locations, including thrust bearings. Thus the bearing thrust load must also be carried by the damper.

The damper test rig described here (fig. 39) was designed to accommodate dampers capable of high radial loads and amplitudes, while also carrying a thrust load. Maximum capabilities of the rig are

Speed, rpm	10 000
Damper radial amplitude, mm	0.5
Rotating load, kN	22
Thrust load, kN	4.4
Damper diameter, mm	200
Damper length, mm	110

Power is provided by an 11-kW variable-speed electric motor driving through a poly-V belt to the shaft of the test rig. The shaft is mounted in duplex ball bearings at each end; the bearings are supported by the test damper at one end and rigidly at the other end. The test damper is loaded radially by imbalance in a disk at the end of the shaft. A pneumatic cylinder provides the thrust load. Shaft and damper amplitudes are measured by eddy-current probes; damper load is measured by quartz load washers. The data are processed by a digital vector filter and online computer for conversion into stiffness and damping coefficients.

The rig has been fully assembled with a solid setup piece in place of a test damper. It has been run to full speed with no imbalance applied. All rotating parts had been previously balanced in a balancing machine prior to assembly in the rig. Observation of the shaft orbits on oscilloscopes showed no detectable increase in amplitude as speed was increased, indicating that the initial balance was excellent. It is anticipated that a short shakedown period will be needed before the rig is ready to receive a test damper. Runs will be made with imbalance applied in order to verify rotor response predictions.

This unique test facility is expected to prove extremely valuable in qualifying new damper designs for gas turbines engines and other high-speed rotating machinery.

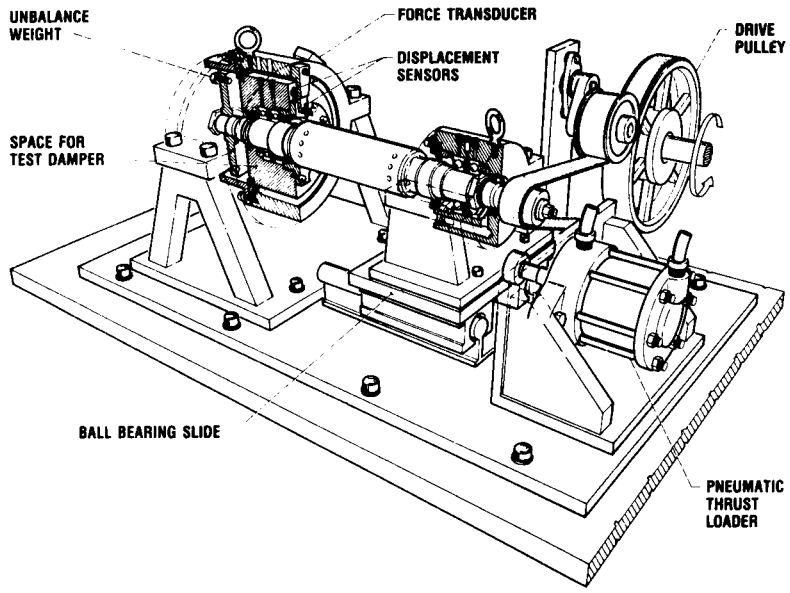

Figure 39.—High-load and -thrust bearing damper rig.

Researchers: D.P. Fleming and M.P. Doherty (NASA Lewis).

Vibration and Control of a Flexible Rotor Supported by Magnetic Bearings

There are many papers on the subject of magnetic bearings. These papers are divided into two categories. One is the use of magnetic bearings taking the place of contacting bearings. The other covers the use of *noncontact actuators for active vibration control.* The present work deals with both categories, namely, active vibration control of flexible rotors supported by magnetic bearings. By using a finite element method for the mathematical model of a flexible rotor, the author has formulated the eigenvalue problem taking into account the interaction between a mechanical system of the flexible rotor and an electrical system of the magnetic bearings and the controller. For the sake of simplicity, gyroscopic effects were disregarded. This formulation has been adapted to a general flexible rotor-magnetic bearing system and applied to a test rig. Controllability with and without collocation (sensors and actuators located at the same distance along the rotor axis) is discussed for the higher order flexible modes of the test rig. It was concluded that it is necessary to add additional active control loops for the higher flexible modes, even in the case of collocation. Then, it is also possible to stabilize for cases without collocation by means of this method.

Table VI lists the eigenvalues of the flexible rotor-magnetic bearing control system with collocation in the ideal case. The real part of all eigenvalues is negative, therefore, every mode is stable. However, the roots of the higher modes approach the imaginary axis (the absolute values of the real parts are very small). This means that it may be difficult to pass through higher critical speeds even in the case of collocation.

Table VII shows the increased stability of the higher modes with collocation and additional velocity feedback loops. In this case, the real parts have larger negative values; thus, damping is greater.

Table VIII shows the eigenvalues without collocation (the experimental case). The real parts of the fourth, fifth, and sixth eigenvalues are positive; thus, these modes are unstable. Improvement of the damping characteristics at these modes is needed in addition to the velocity feedback.

The root locus of eigenvalue analysis in this experiment without collocation is shown in figure 40. It is found for the analysis, and verified by experiment, that

TABLE VI.—EIGENVALUES WITH COLLOCATION

Eigenvalues		Frequency, Hz
Real	Imaginary	
−0.22273D−2	0.36128D+5	5750.0
−.22359D−1	.15725D+5	2502.7
−.70242D−1	.12784D+5	2034.6
−.57519D+0	.59381D+4	945.1
−.89774D+1	.29159D+4	464.1
−.22630D+2	.20626D+4	328.3
−.64734D+2	.94692D+3	150.7
−.47460D+2	.66731D+3	106.2
−.82129D+2	.15805D+3	25.2
−.94146D+2	.15287D+3	24.3
−.49705D+1	.12235D+3	19.5

TABLE VII.—EIGENVALUES WITH COLLOCATION IN ADDITION TO VELOCITY FEEDBACK

Eigenvalues		Frequency, Hz
Real	Imaginary	
−0.46911D+3	0.11555D+4	183.9
−.59602D+3	.91103D+3	145.0
−.14625D+3	.36865D+3	58.7
−.28629D+3	.34515D+3	54.9
−.46764D+0	.13729D+3	21.9

TABLE VIII.—EIGENVALUES WITHOUT COLLOCATION

Eigenvalues		Frequency, Hz
Real	Imaginary	
−0.16181D+2	0.20101D+4	319.9
−.74842D+2	.86925D+3	138.3
−.71604D+2	.62756D+3	99.9
−.11111D+3	.17393D+3	27.7
−.12722D+3	.15032D+3	23.9
−.65155D+1	.10677D+3	17.0

the characteristic of the fourth mode is improved by active velocity feedback loops; the unstable fourth root goes to the stable region. In this figure, the arrow indicates the direction of increasing velocity feedback. Doubling the feedback from the first trial value improves stability of both the fourth and fifth modes, but further increases degrade stability. Any amount of velocity feedback seems to reduce the stability of the first two modes; however, they are still well within the stable region.

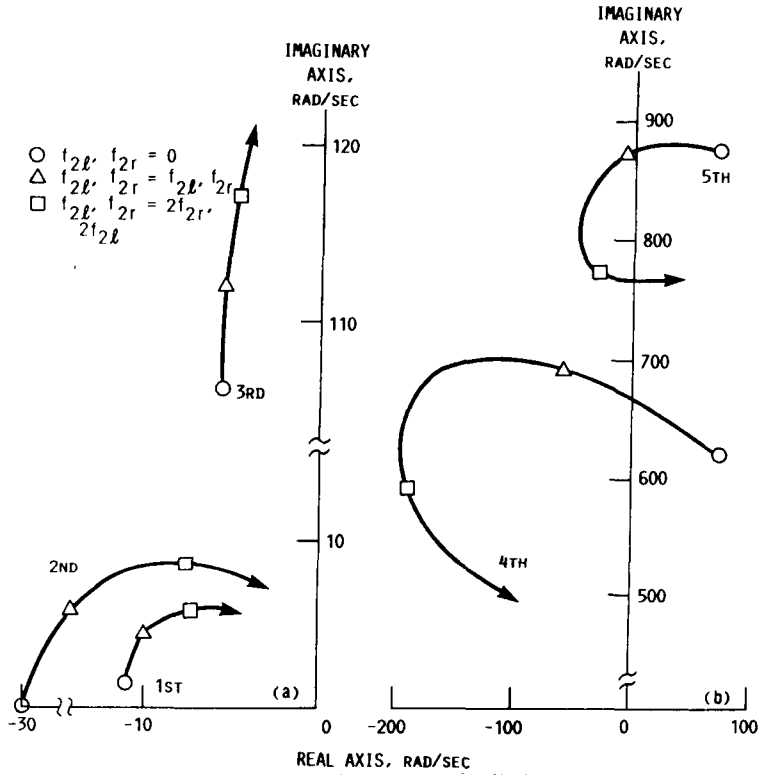

(a) Modes 1 to 3.
(b) Modes 4 and 5.

Figure 40.—Root loci without collocation in addition to velocity feedback.

Researchers: K. Nonami and D.P. Fleming (NASA Lewis).

Active Control of Rotor Vibrations

Jet engine shaft vibrations are suppressed by passive devices such as squeeze film dampers. Research is being performed to replace or supplement these by active dampers, to reduce engine weight and produce more predictable and reliable damping. The research reported here uses piezoelectric pushers for actuators in active dampers, because of their light weight, compactness, and low-voltage.

This research showed that

(1) Standard control theories such as optimal, pole placement, and velocity feedback could be applied to the prescribed displacement characteristics of piezoactuators.

(2) The pusher could yield between 50- and 80-lb-sec/in. damping as determined by comparison of test and simulation results. The test rig is shown in figure 41, and the accompanying vibration reduction plots are shown in figure 42.

(3) A narrow bandpass tracking filter was required to suppress instabilities of the control system. The method was effective except when the rotor speed was just below a critical speed, in which case an instability occurred.

The ensuing strategy for developing the piezoelectric-actuator active damper was to

(1) Determine, by computer simulation, what piezopusher specifications (force, stroke, stiffness) would be required for effective control of vibration in various jet engines.

(2) Identify the cause of the electromechanical instability problem and develop solutions.

(3) Work with the piezopusher manufacturer (Burleigh, Inc.) to develop more powerful pushers.

Task (1) was approached by performing rotordynamics simulations on the T700, T64, and T55 engines.

Figure 43 shows the first mode shape, unbalance response plot, and pusher internal displacement for a typical T700 simulation run. The T700 falls in the category "small general aviation engine (SGAE)" according to criteria proposed in Bhat, S.T., et al. (Analysis of High Load Dampers. (5779–10, Pratt and Whitney; NASA Contract NAS3–22518). NASA CR–165503, 1981).

Model	Maximum rotor, lb	Maximum rotor, in.	Maximum speed, rpm
SGAE	150	70	20 000
T700	21	38	[a]16 000

[a]Service.

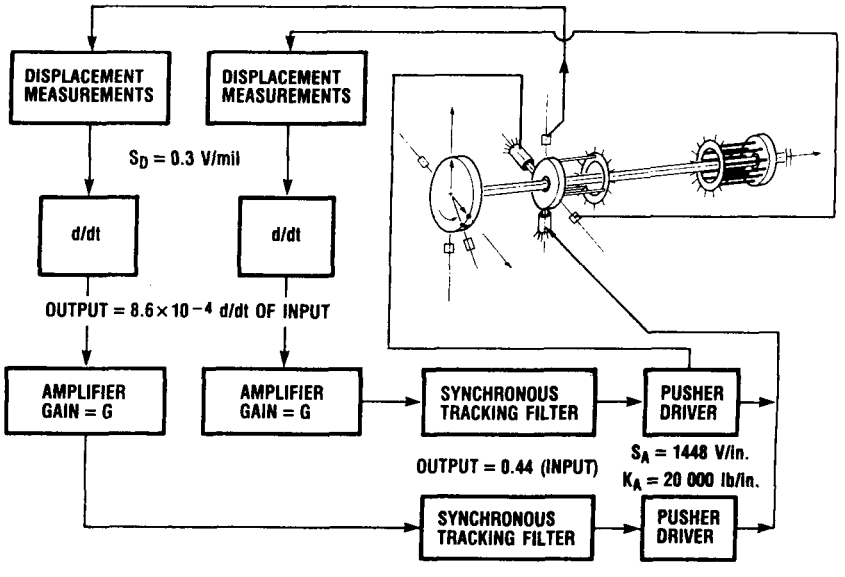

Figure 41.—Rotor test rig with active damping feedback loop using piezoelectric pusher actuators.

A comparison of the T700 results to the maximum acceptable vibration proposed in the Bhat report follows:

Model	Maximum turbine vibration,[a] mils/oz in.	Maximum damper vibration,[a] mils/oz in.
SGAE	5.0	4.5
T700	.7	.5

[a]At operating speed.

The T700 results are for an active damper value of 100 lb-sec/in. which produces a pusher internal displacement of 8 mils/oz in. and force of 200 lb/oz in. Although the pusher displacement requirement exceeds the 2- to 3-mils limit of existing pushers, larger displacements can be obtained by stacking piezopushers in series. Similar simulations are currently being performed on the T64 and T55 engines.

The problem addressed in task (2) arose when the test rig response had high-frequency pulses. Those instabilities range from 1000 to 9000 Hz and are caused by the phase change in the differentiators and piezopushers. If the total phase lag becomes greater than 90° the active damping becomes negative and an instability may occur. Insertion of low pass filters into the feedback loop is not a certain solution since they also have phase lag.

A narrow bandpass, synchronous tracking filter stabilizes the system except when the rotor speed approaches a critical speed in which case the 90° phase shift of the filter causes the critical speed to become unstable. The current strategy being developed is to use a combined approach of low pass filtering, phase lead circuitry, mechanical natural frequency shifting, and mechanical isolation to stabilize the closed-loop system.

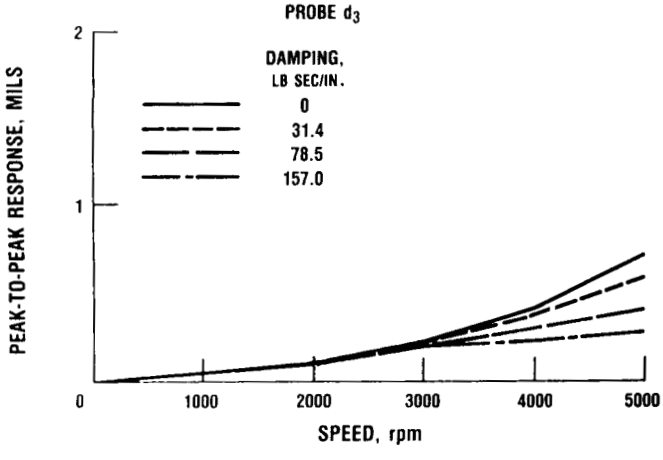

Figure 42.—Vibration reduction achieved with increasing active damping. Experimental data from probe D3.

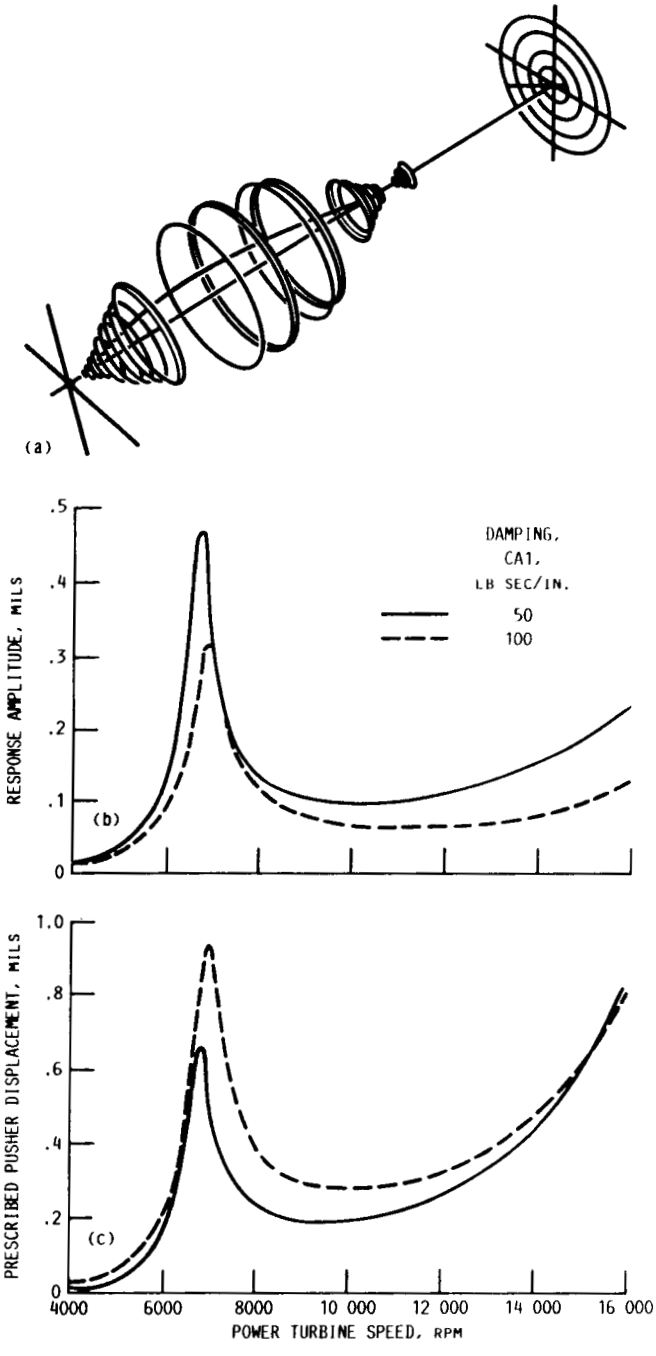

(a) Mode shape.
(b) Unbalance response.
(c) Pusher displacement.

Figure 43.—T700 power turbine simulation results.

Task (3) was initiated by meeting with a piezoelectric pusher manufacturer, the primary investigator, and Burleigh personnel (Burleigh, Inc.) and discussing improvements required in the pushers for effective active vibration control. These included increased force, stroke, frequency response, linearity, and high-temperature survivability. Burleigh recently loaned us two "increased stiffness" prototype pushers and has given instructions on changing the frequency response characteristics of the pusher's amplifier-driver.

Researchers: A.F. Kascak (AVSCOM), A.B. Palazzolo (Texas A&M), G.T. Montague (Sverdrup), and R. Lin (Texas A&M).

Appendix—Researchers

Abdallah, A.A. ..... Case Western Reserve University, Cleveland, Ohio
Akl, F.A. ..... Ohio University, Athens, Ohio
August, R. ..... Sverdrup Technology, Inc., NASA Lewis Research Center Group, Cleveland, Ohio
Black, G. ..... General Electric Company, Cincinnati, Ohio
Brush, A.S. ..... Sverdrup Technology, Inc., NASA Lewis Research Center Group, Cleveland, Ohio
Chung, C.L. ..... Carnegie-Mellon University, Pittsburgh, Pennsylvania
Dellacorte, C. ..... NASA Lewis Research Center, Cleveland, Ohio
Desa, S. ..... Carnegie-Mellon University, Pittsburgh, Pennsylvania
Doherty, M.P. ..... NASA Lewis Research Center, Cleveland, Ohio
Ellis, G.K. ..... Institute for Computational Mechanics in Propulsion (ICOMP), NASA Lewis Research Center, Cleveland, Ohio
Fleming, D.P. ..... NASA Lewis Research Center, Cleveland, Ohio
Gallardo, V. ..... General Electric Company, Cincinnati, Ohio
Guptill, J.D. ..... NASA Lewis Research Center, Cleveland, Ohio
Huckelbridge, A.A. ... Case Western Reserve University, Cleveland, Ohio
Janetzke, D.C. ..... NASA Lewis Research Center, Cleveland, Ohio
Kascak, A.F. ..... U.S. Army Aviation Research and Technology Activity—AVSCOM, NASA Lewis Research Center, Cleveland, Ohio
Kaza, K.R.V. ..... NASA Lewis Research Center, Cleveland, Ohio
Kielb, R.E. ..... NASA Lewis Research Center, Cleveland, Ohio
Kiraly, L.J. ..... NASA Lewis Research Center, Cleveland, Ohio
Lawrence, C. ..... NASA Lewis Research Center, Cleveland, Ohio
Lin, R. ..... Texas A&M University, College Station, Texas
Mehmed, O. ..... NASA Lewis Research Center, Cleveland, Ohio
Montague, G.T. ..... Sverdrup Technology, Inc., NASA Lewis Research Center Group, Cleveland, Ohio
Morel, M. ..... Ohio University, Athens, Ohio
Murthy, D.V. ..... The University of Toledo, Resident Research Associate at NASA Lewis Research Center, Cleveland, Ohio
Narayanan, G.V. ..... Sverdrup Technology, Inc., NASA Lewis Research Center Group, Cleveland, Ohio
Nonami, K. ..... Chiba University, Chiba, Japan
North, C.M. ..... Rose-Hulman Institute of Technology, Terre Haute, Indiana
Palazzolo, A.B. ..... Texas A&M University, College Station, Texas
Ramsey, J.K. ..... NASA Lewis Research Center, Cleveland, Ohio
Reddy, T.S.R. ..... The University of Toledo, Resident Research Associate at NASA Lewis Research Center, Cleveland, Ohio
Rodriguez, H. ..... University of Michigan, Ann Arbor, Michigan
Rohn, D.A. ..... NASA Lewis Research Center, Cleveland, Ohio
Sirocky, P.J. ..... Sverdrup Technology, Inc., NASA Lewis Research Center Group, Cleveland, Ohio
Smolinski, P. ..... University of Pittsburgh, Pittsburgh, Pennsylvania
Srivastava, R. ..... Georgia Institute of Technology, Atlanta, Georgia
Steinetz, B. ..... NASA Lewis Research Center, Cleveland, Ohio
Williams, M. ..... Purdue University, West Lafayette, Indiana

Bibliography

August, R.; and Kaza, K.R.V.: Vibration and Flutter Characteristics of the SR7L Large-Scale Propfan. NASA TM–100272, 1988.

August, R.; and Kaza, K.R.V.: Vibration, Performance, Flutter and Forced Response Characteristics of a Large-Scale Propfan and Its Aeroelastic Model. AIAA Paper 88–3155, July 1988. (NASA TM–101322).

Ellis, G.K.: Implementing Direct, Spatially Isolated Problems on Transputer Networks. NASA TM–101297, 1988.

Ellis, G.K.: User's Manual for the Two-Dimensional Transputer Graphics Toolkit. NASA TM–100974, 1988.

Ellis, G.K.: Two-Dimensional Graphics Tools for a Transputer Based Display Board. NASA TM–100820, 1988.

Ellis, G.K.: Distributed Computation of Graphics Primitives on a Transputer Network. NASA TM–l00814, 1988.

Griffin, J.H.: Bladed Disk Vibration. NASA CR–181203, 1987.

Kaza, K.R.V., et al.: Aeroelastic Response of Metallic and Composite Propfan Models in Yawed Flow. AIAA Paper 88–3154, July 1988. (NASA TM–100964).

Lawrence, C.; and Huckelbridge, A.A.: Characterization of Damped Structural Connections for Multi-Component Systems. NASA TM–100801, 1988.

Lawrence, C.: Parameter Identification Methods for Improving Structural Dynamic Models. NASA TM–100812, 1988.

Lewis Structures Technology—1988, Vol. 1—Structural Dynamics. NASA CP–3003 VOL–1, 1988.

Mehmed, 0.; and Murthy, D.V.: Experimental Investigation of Propfan Aeroelastic Response in Off-Axis Flow with Mistuning. AIAA Paper 88–3153, July 1988. (NASA TM–101320).

Montague, G.T.; and Kielb, R.E.: Test Facilities of the Structural Dynamics Branch of NASA Lewis Research Center. NASA TM–100800, 1988.

Murthy, D.V.; and Kaza, K.R.V.: A Semianalytical Technique for Sensitivity Analysis of Unsteady Aerodynamic Computations. 29th Structures, Structural Dynamics and Materials Conference, Part 3, AIAA, 1988, pp. 1307–1316. (NASA TM–100810).

Murthy, D.V.; and Kaza, K.R.V.: A Computational Procedure for Automated Flutter Analysis. NASA TM–100171, 1987.

Nonami, K.: Vibration and Control of Flexible Rotor Supported by Magnetic Bearings. NASA TM–100888, 1988.

Palazzolo, A.B., et al.: Active Control of Transient Rotordynamic Vibration by Optimal Control Methods. ASME Paper 88–GT–73, June 1988.

Quinn, R.D.; Chen, J.L.; and Lawrence, C.: Redundant Manipulators for Momentum Compensation in a Micro-Gravity Environment. AIAA Guidance, Navigation and Control Conference, Part 2, AIAA, 1988, pp. 581–587.

Ramsey, J.K.; and Kielb, R.E.: A Computer Program for Calculating Unsteady Aerodynamic Coefficients for Cascades in Supersonic Axial Flow. NASA TM–100204, 1987.

Reddy, T.S.R.; Srivastava, R.; and Kaza, K.R.V.: The Effects of Rotational Flow, Viscosity, Thickness, and Shape on Transonic Flutter Dip Phenomena. 29th Structures, Structural Dynamics and Materials Conference, Part 2, AIAA, 1988, pp. 1096–1108. (NASA TM–100811).

Rohn, D.A.; Lawrence, C.; and Brush, A.S.: Microgravity Robotics Technology Program. NASA TM–100898, 1988.

Smalley, A.J.; Baldwin, R.M.; and Schick, W.R.: Spray Automated Balancing of Rotors: Methods and Materials. NASA CR–182151 (also, AVSCOM–TR–88–0–018), Aug. 1988.

Stefko, G.L.; and Jeracki, R.J.: Porous Wind Tunnel Corrections for Counterrotation Propeller Testing. AIAA Paper 88–2055, May 1988. (NASA TM–100873).

Structural Dynamics Branch Research and Accomplishments for Fiscal Year 1987. NASA TM–100279, 1988.

Williams, M.H.: Aeroelastic Effects of Alternate Blade Sweep on Advanced Propfan Rotor. ASME Paper 87–WA/Aero 8, Dec. 1987.

Yousef, S.; and Akl, F.: Forced Vibration Analysis of a Slender Stack Equipped with Sliding and Pendulum Impact Dampers. Developments in Theoretical and Applied Mechanics, Vol. 14, S.S.Y. Wang, et al., eds., University of Mississippi, 1988.

NASA
National Aeronautics and Space Administration

Report Documentation Page

1. Report No.	2. Government Accession No.	3. Recipient's Catalog No.
NASA TM-101406		

4. Title and Subtitle	5. Report Date
Structural Dynamics Branch Research and Accomplishments for FY 1988	April 1989
	6. Performing Organization Code

7. Author(s)	8. Performing Organization Report No.
	E-4498
	10. Work Unit No.
	505-63-1B

9. Performing Organization Name and Address	11. Contract or Grant No.
National Aeronautics and Space Administration Lewis Research Center Cleveland, Ohio 44135-3191	
	13. Type of Report and Period Covered
	Technical Memorandum

12. Sponsoring Agency Name and Address	14. Sponsoring Agency Code
National Aeronautics and Space Administration Washington, D.C. 20546-0001	

15. Supplementary Notes

16. Abstract

This publication contains a collection of fiscal year 1988 research highlights from the Structural Dynamics Branch at NASA Lewis Research Center. Highlights from the branch's major work areas—Aeroelasticity, Vibration Control, Dynamic Systems, and Computational Structural Methods—are included in the report as well as a complete listing of the FY 88 branch publications.

17. Key Words (Suggested by Author(s))	18. Distribution Statement
Aeroelasticity Vibration control Dynamic systems Computational structural methods	Unclassified – Unlimited Subject Category 39

19. Security Classif. (of this report)	20. Security Classif. (of this page)	21. No of pages	22. Price*
Unclassified	Unclassified	47	A03

NASA FORM 1626 OCT 86

*For sale by the National Technical Information Service, Springfield, Virginia 22161

National Aeronautics and
Space Administration

Lewis Research Center
Cleveland, Ohio 44135

SECOND CLASS MAIL

ADDRESS CORRECTION REQUESTED

Official Business
Penalty for Private Use $300

Postage and Fees Paid
National Aeronautics and
Space Administration
NASA-451

NASA

Report Documentation Page

Report No.	2. Government Accession No.	3. Recipient's Catalog No.
NASA TM-101406		

Title and Subtitle

Structural Dynamics Branch Research and Accomplishments for FY 1988

5. Report Date: April 1989

6. Performing Organization Code:

Author(s)

8. Performing Organization Report No.: E-4498

10. Work Unit No.: 505-63-1B

Performing Organization Name and Address

National Aeronautics and Space Administration
Lewis Research Center
Cleveland, Ohio 44135-3191

11. Contract or Grant No.:

13. Type of Report and Period Covered: Technical Memorandum

Sponsoring Agency Name and Address

National Aeronautics and Space Administration
Washington, D.C. 20546-0001

14. Sponsoring Agency Code:

Supplementary Notes

Abstract

~~This publication contains a collection of~~ fiscal year 1988 research highlights from the Structural Dynamics Branch at NASA Lewis Research Center. Highlights from the branch's major work areas are described. Aeroelasticity, Vibration Control, Dynamic Systems, and Computational Structural Methods are included ~~in the report~~ as well as a complete listing of the FY-88 branch publications.

Key Words (Suggested by Author(s))	18. Distribution Statement
Aeroelasticity Vibration control Dynamic systems Computational structural methods	Unclassified – Unlimited Subject Category 39

Security Classif. (of this report)	20. Security Classif. (of this page)	21. No of pages	22. Price*
Unclassified	Unclassified	47	A03

*For sale by the National Technical Information Service, Springfield, Virginia 22161